Tectonophysics 838 (2022) 229470

Contents lists available at ScienceDirect

Tectonophysics

journal homepage: www.elsevier.com/locate/tecto

3D velocity-depth model from multichannel seismic in the Dinaric foredeep of the Gulf of Trieste (Adriatic Sea), at the NE edge of Adria plate

Michela Dal Cin [a,b,*], Gualtiero Böhm [a], Martina Busetti [a], Stefano Picotti [a], Fabrizio Zgur [a], Angelo Camerlenghi [a]

[a] National Institute of Oceanography and Applied Geophysics – OGS, I-34010 Sgonico, Trieste, Italy
[b] Department of Mathematics and Geosciences, University of Trieste, I-34128 Trieste, Italy

ARTICLE INFO

Keywords:
Adria plate
Dinaric foredeep
Southeastern distal Alpine foreland
Karst Thrust
Adria-Eurasia collisional plate boundary
Multichannel reflection seismic
Traveltime reflection tomography
Depth seismic imaging
3D velocity-depth model

ABSTRACT

The Gulf of Trieste (GT), northeastern Adriatic, sits at the rigid edge of the Adria microplate representing the foreland of the adjoining Meso-Cenozoic External Dinarides and Southeastern Alps. The Adria-Eurasia plate boundary extends along the GT eastern coastline, depicted by the Karst Thrust, outer ramp of the SW-verging Dinarides. This separates the Cretaceous-Paleogene carbonates outcropping hundreds of meters on the Karst Plateau (hanging-wall) from their counterparts buried in the eastern gulf. Although the thrust has no evidence of historical and instrumental seismicity, a detailed seismic velocity field is needed to quantify reliable geometries in the foredeep, embedded in a tectonically active area where Adria is moving NNW-ward. Availability of a newly acquired marine multichannel seismic dataset, allowed us to provide the first well-constrained 3D P-wave velocity and depth model in the footwall of the Karst Thrust. Two iterative techniques, traveltime reflection tomography and depth seismic imaging, were applied on the data surveying the Dinaric foredeep. Our findings provide mean velocity values of 1700 m/s for the Quaternary sediments, 2900 m/s for the upper Eocene flysch turbidites, 4500 m/s for the lower flysch, 5000 m/s for the upper carbonates. The maximum flysch unit thickness results in about 1500 m and the top carbonates depth reaches about 1600 m below sea level, 1.7 km offshore Trieste, revealing the thrust is responsible for a minimum 1600–1800 m vertical throw. This study provides benefits for Adria geodynamic models and give new constraints for the geological and tectonic setting assessment, in a region settled over a currently active continental margin.

1. Introduction

The northeastern edge of the Adria microplate is settled in a complex structural framework, as it lies at the southern junction of the Meso-Cenozoic SW-verging External Dinarides and S-verging Southeastern Alps, originated by Adria-Eurasia continental collision (Dewey et al., 1989; Carminati and Doglioni, 2012; Faccenna et al., 2014 and references therein). This rigid corner of the Adria block, comprising the Venetian-Friulian plain and the northern Adriatic Sea, represents the eastern foredeep and southeastern distal foreland of Alpine and Dinaric thrust-fold belts, respectively (inset - Fig. 1; e.g., Burrato et al., 2008; Galadini et al., 2005; Placer et al., 2010; Zanferrari et al., 2008).

In the frame of the Mediterranean geodynamic evolution, the Adria microplate has a prominent role due to its subduction to the E (Dinaric) and W (Apenninic) and northward indentation into the Alpine orogen (e.g., Handy et al., 2015; Schmid et al., 2004), that induce varying styles of crustal deformation along its margins. The ongoing NNW-ward Adria motion relative to Eurasia, up to 4 mm/yr (Vrabec and Fodor, 2006; Weber et al., 2010), is accommodated by active compressive tectonics resulting in deformation of Pleistocene deposits and present-day seismicity at the frontal ramps of the Southern Alpine domain (Galadini et al., 2005; OGS, 2017; Patricelli and Poli, 2020; Poli et al., 2015; Rovida et al., 2020; Viscolani et al., 2020). The northernmost Dinaric fault system shows recent displacement along NW-SE striking structures (as Idrija and Raša faults) reactivated in dextral transcurrent kinematics and responsible for historical and instrumental earthquakes (Fitzko et al., 2005; Vičič et al., 2019). Neotectonic transcurrent and transpressional deformation is observed also within the Dinaric-Alpine

Abbreviations: CAT3D, Computer Aided Tomography for 3D models; DMG, Depth Migrated Gathers; DSI, Depth Seismic Imaging; FDCP, Friuli-Dinaric Carbonate Platform; GT, Gulf of Trieste; PSDM, Pre-Stack Depth Migration; TRT, Traveltime Reflection Tomography.

* Corresponding author at: National Institute of Oceanography and Applied Geophysics – OGS, I-34010 Sgonico, Trieste, Italy.
E-mail address: mdalcin@ogs.it (M. Dal Cin).

https://doi.org/10.1016/j.tecto.2022.229470
Received 29 September 2021; Received in revised form 16 June 2022; Accepted 29 June 2022
Available online 12 July 2022

foredeep in the easternmost Friulian plain (Accaino et al., 2019; Burrato et al., 2008).

It is well established that understanding the geodynamic evolution of tectonic plates and associated geohazards relies in the integration of studies examining both deep and shallow Earth's processes. Geophysical research on mantle (e.g., Guidarelli et al., 2017; Stipčevič et al., 2011) and crustal (e.g., Castellarin et al., 2006; TRANSALPWorking Group, 2002) structures contributed to improve the knowledge on the polyphasic architecture and deformation history of the region (e.g., Handy et al., 2015; Schmid et al., 2004). Although the surface expression of

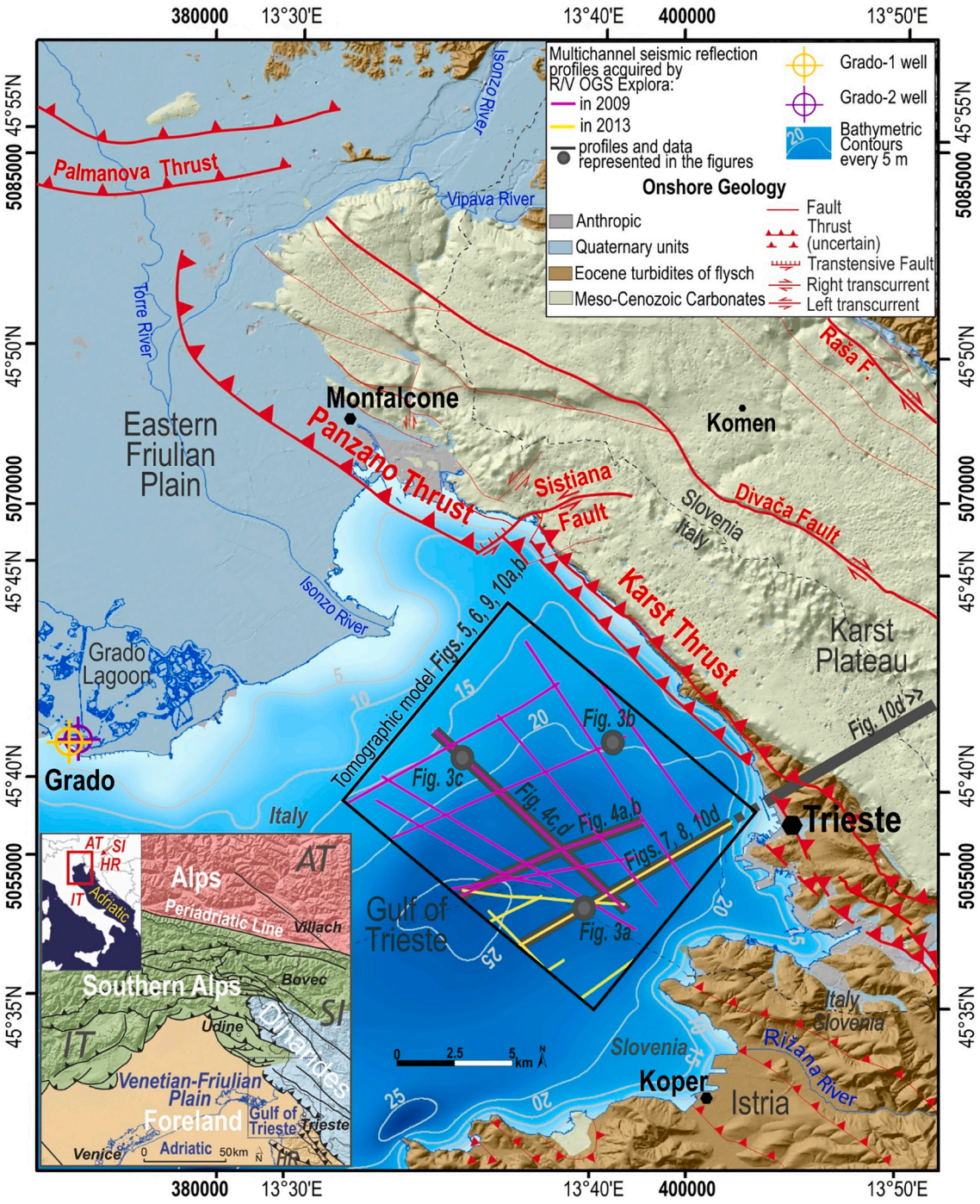

Fig. 1. Map of the eastern Gulf of Trieste with the area (black rectangle) in which the tomographic 3D velocity depth model was calculated. The analyzed multichannel seismic reflection profiles belong to the 2009 and 2013 surveys (purple and yellow lines, respectively), collected onboard the R/V OGS Explora. The purple and orange circles show position of Grado geothermal wells. Bathymetry with 50 m cells, gridding performed by Zampa (2020) by using grids from Italy, Slovenia (Trobec et al., 2018) and Croatia (EMODnet Digital Bathymetry, 2018). Onshore geology is represented for Friulian Plain and Italian Karst Plateau (GEO-CGT, 2013), Slovenian Karst Plateau (Jurkovšek et al., 2016), Istria (Placer et al., 2010). Digital Elevation Model compiled for Italy (10 m cells; IRDAT-FVG, 2017), Slovenia (10 m cells; Arso, 2017) and Istria (25 m cells; EU-DEM, 2017). Inset: chains and foreland domains of the region surrounding the Gulf of Trieste. Inset: chains and foreland domain of the region with main tectonic lineaments (Burrato et al., 2008; GEO-CGT, 2013; Galadini et al., 2005; Jurkovšek et al., 2016; Placer et al., 2010; Zanferrari et al., 2008). Map compiled in ArcGIS® software by Esri, datum WGS84, projection UTM33. (For interpretation of the references to colour in this figure legend, the reader is referred to the web version of this article.)

deformation gives insights into the mantle convection processes, reconstructing complex crustal geometries in highly deformed plate margins and subducting microplates, as for the Adria plate, remains a challenging task. A variety of different geological and geophysical data is required, and difficulties generally rely in their different time and space distribution and resolution, along with the feasibility of their combined analysis (e.g. Faccenna et al., 2014; Le Breton et al., 2017; Brancolini et al., 2019).

In the past decades, tectono-stratigraphic evolution of the upper crust in foreland domain has been mainly reconstructed through oil industry (ENI) wells and medium-deep penetration multichannel seismic (MCS) data, collected in the 1970s and 1980s in the Venetian-Friulian plain (e.g. Fantoni et al., 2002; Fantoni and Franciosi, 2010; Nicolich et al., 2004). Over the central part of the northern Adriatic, the deep crustal structure of the foreland domain was explored by the marine active seismic CROP95-M18 profile, recorded in 1995 (Finetti and Del Ben, 2005; Scrocca et al., 2003). The northeastern tip of Adria plate in submarine setting, namely the Gulf of Trieste (GT), has been only recently surveyed thanks to the collection of a dense network of medium-high resolution MCS reflection data by the National Institute of Oceanography and Applied Geophysics – OGS (Busetti et al., 2010a, 2010b, 2013; Zgur et al., 2010, 2013). This approach unlocked a window into the crustal deformation of the Adria basin close to the Dinaric-Alpine intersection, where the present-day structural style is mainly determined by the rheological contrast between the ductile Eocene turbiditic deposits of flysch and their rigid NE-ward flexured Cretaceous-Paleogene carbonate bedrock. The eastern sector of the gulf represents the footwall of the outermost front of the Dinarides orogen, that is the Karst Thrust extending along the eastern rocky coastal area (Fig. 1). The hanging-wall of the thrust is represented by the Classical Karst Plateau, rising some hundreds of meters above sea level on the adjacent eastern onland (Busetti et al., 2010a, 2010b, 2013). While the geodynamic reconstruction of Adria microplate is beyond our aims, the availability of this latest seismic dataset in the GT offers today the novel and unique possibility to extract quantitative geophysical parameters and geometries of the buried Adria upper crustal structure in the proximity of a highly deformed collisional domain.

We perform advanced tomographic techniques, on MCS reflection profiles in the eastern GT, involving Traveltime Reflection Tomography (TRT) (Böhm et al., 1999, 2000; Vesnaver and Böhm, 2000) and Depth Seismic Imaging (DSI) (Yilmaz, 2001), to propose the first well-constrained 3D P-wave velocity-depth model of the External Dinarides foredeep.

The same methodologies have been successfully applied to determine accurate seismic velocities and reconstruct the structure at depth in presently active convergent plate margins over the world. Some examples concern the Nankai Trough where the Philippine Sea Plate is subducting beneath the Eurasian Plate (Park et al., 2002), the frontal ramp of the Main Himalayan Thrust (Liu et al., 2020), the Kodiak fault zone of the Alaskan convergent plate boundary between the Pacific and North American plates (Krabbenhoeft et al., 2021).

Our aim is to estimate the seismic velocities of three main sedimentary units (Plio-Quaternary sediments, Eocene flysch and Cretaceous-Paleogene carbonates) and the reconstruction in depth of their top surfaces. Although the fault plane of the Kast Thrust is not imaged by data, the accurate reconstruction of the seismic velocity field in its footwall is crucial to quantify its significant vertical throw. This information can be extrapolated throughout the eastern Friulian plain, where industrial seismic data (e.g., Merlini et al., 2002; Nicolich et al., 2004) have lower resolution and spatial distribution, but where lithological and tectonic setting is analogous. This is represented by the Dinaric foredeep delimited to the E by the Panzano and Palmanova thrusts (Fig. 1), that are the Karst Thrust's northward external Dinaric frontal ramp prosecution, with NW-SE orientation and WSW-ENE lateral ramps and with the Palmanova Thrust recently reactivated by the Neoalpine orogeny phase (Merlini et al., 2002; Zanferrari et al., 2013). Neither historical nor instrumental seismological activity has been related to the Karst Thrust, but this is located in a tectonically active region (e.g., Meletti et al., 2021; Rebez et al., 2016; Santulin et al., 2017; Visini et al., 2021). Therefore, the outcomes of our analysis can provide valuable input for enhancing neotectonics research in a strongly urbanized and industrialized coast. The coast of the eastern gulf hosts tree major shipping harbors that, from N to S, are: Monfalcone (it serves also as high tonnage shipyard) Trieste and Koper. The Free Port of Trieste (e.g., Memorandum of London, 1954; Treaty of Osimo, 1975) is the main oil terminal in the Mediterranean. Both the Trieste and Koper harbors are international hubs for trade with central and eastern Europe and they represent major blue-economy infrastructures, being the first ports, in Italy and Slovenia respectively, for total cargo and rail traffic to major European destinations through the TEN-T Baltic-Adriatic and Mediterranean core network corridors (European Commission, 2021; Port Network Authority of the Eastern Adriatic Sea, 2021). Moreover, this study can give a contribution in understanding wide scale processes occurring in a complex tectonic and geodynamic patchwork, where Adria is currently sliding along inherited Dinaric lineaments and it is colliding against the Alps.

2. Geological background

The GT is located in the northeastern Adriatic Sea and it is bounded to the N by the eastern Friulian Plain (Italy), to the E by the Classical Karst Plateau and to the S by the Istria peninsula (Slovenia, Croatia). It represents the foredeep of the adjacent External Dinarides and the distal foreland of the Southeastern Alpine chain (Busetti et al., 2010a, 2010b, 2013; Nicolich et al., 2004) merging to the north and NW-SE and E-W oriented, respectively (Fig. 1).

During the Mesozoic, a rifting stage affected the Upper Triassic Dolomia Principale carbonate platform and allowed the aggradation of the Mesozoic-Paleogene Friuli-Dinaric Carbonate Platform (FDCP) (Cati et al., 1987; Fantoni et al., 2002). Onland investigation described the carbonate platform units outcropping on the Karst Plateau (see GEOCGT, 2013; Jurkovšek et al., 2016 and refences therein) and buried under the Friulian Plain (Cati et al., 1987; Nicolich et al., 2004; Zanferrari et al., 1982, 2008, 2013).

A major offshore geophysical investigation took place recently, with collection of a dense network of MCS reflection data by the R/V OGS Explora (Busetti et al., 2010a, 2010b; Busetti et al., 2013; Zgur et al., 2010, 2013), (Fig. 1).

Moreover, core drilling operations at geothermal sites (e.g., Della Vedova et al., 2014), seismological (e.g., OGS, 2017) and secular-term geodetic observations (e.g., Braitenberg et al., 2006) have been carried out over the last four decades.

These geophysical investigations evidenced the following main characteristics:

1. **Polyphase tectonics and sedimentation.** Analysis of seismic data revealed polyphase tectonics of the area, since the Late Mesozoic (Busetti et al., 2013). The Late Cretaceous-Paleogene Dinaric compressional phase produced a complex fold-thrust system, NW-SE oriented. The related foredeep migrated progressively SW-ward, involving, in the final stage, the eastern part of the GT. Here, the carbonate platform was flexured E-ward and the turbiditic sediments of flysch filled the basin during Eocene (Busetti et al., 2010a, 2010b, 2013). Two main steps of deposition can be distinguished. The first allowed thicker sequence of turbidities infill the depocenter, the second led to sedimentation of a thinner sealing package. The entire unit is W-ward pinching out on the peripheral bulge of the system (Busetti et al., 2010a, 2010b). The top of the Paleogene carbonates is intercepted by the Grado-1 and Grado-2 geothermal wells at a depth of 616.5 and 630.0 m, respectively, overlying the Cretaceous limestones occurring at a depth of 1006 and 1004 m. At the borehole sites, the thickness of the flysch is about 100 m (e.g., Della Vedova

et al., 2014). The marine regression during the Messinian Salinity Crisis, allowed sub-aerial erosion to shape the top flysch in valleys and ridges (Busetti et al., 2010a, 2010b). In the gulf, sub-areal conditions lasted until the Plio-Quaternary, when marine and continental sediments covered progressively the Messinian unconformity from W to E, draping the easternmost part in the Middle Pleistocene (Busetti et al., 2010a, 2010b; Zecchin et al., 2022). The northern onshore area adjacent to the gulf (Friulian plain) is covered by continental and marine Plio-Quaternary deposits.

2. **Tectonic asset - main faults.** The most external expression of the External Dinarides is represented by the Karst Thrust, running subparallel and near to the Karst coastline. The thrust is limited to the north by the anti-Dinaric (NE-SW) trending left lateral transtensional Sistiana fault and continues towards NW as the Panzano Thrust, with a W-ward offset of about 1–2 km; while it continues SE-ward, in the Slovenian onshore, as the "Črni Kal Thrust" (Busetti et al., 2010a, 2010b; GEO-CGT, 2013; Placer et al., 2010). The Karst Thrust dislocates the carbonates and the flysch with a very important vertical throw. The footwall of the thrust lies in the eastern part of the gulf. The hanging-wall of the Karst Thrust is represented by the Classical Karst Plateau, rising some hundreds of meters above sea level and settled on a wide asymmetric anticline, with NW-SE axis, that brings the outcropping carbonates above the younger Eocene flysch (Busetti et al., 2010a, 2010b).
3. **Neotectonics**. With Adria microplate moving NNW-ward, seismicity occurs in the southeastern Alps and External Dinarides domains (e.g., Meletti et al., 2021; OGS, 2017; Santulin et al., 2017; Visini et al., 2021). Recently, Vičič et al. (2019) discovered swarms and swarm-like seismic sequences happening at depth between 8 and 16 km along the NW-SE oriented strike-slip Raša Fault, that has a geomorphological expression on the Karst Plateau. Furthermore, secular-term geodetic observations of the Karst Plateau, over the last four decades, indicate a regional tilting NW-ward, that has a tectonic origin (Braitenberg et al., 2006). In the GT, neotectonics and reactivation of inherited faults, with dextral transcurrent activity, are suggested in the MCS data by evidence of fluids within the Plio-Quaternary sediments (Busetti et al., 2013; Giustiniani et al., 2022; Vesnaver et al., 2020, 2021a). Fluid migration is probably driven along fault planes towards the seabed, where fluids seepages in the water plumes, metric mud volcanoes and pockmarks occur, as evidenced by high resolution sub bottom profiler/Chirp data (Gordini et al., 2004; Busetti et al., 2019; Vesnaver et al., 2021b). Moreover, geomorphological investigations along the coast highlight recent tectonic movements (Furlani et al., 2011). In particular, in the northeastern coast, the Authors report that the Post-Roman age tidal coastal notches carved in the limestones deepen NW-ward, with a steep downdrop from about 1.2 to 2.3–2.8 m north of the transtensive Sistiana Fault. The displacement possibly occurred in response to creeping, within a regional NW tilting, and it is probably still active today.

3. Multichannel seismic profiles

The analysis performed in this work involved an area of 154 km^2, in the eastern GT (i.e., Dinaric foredeep) covered quite uniformly by 132 km of MCS profiles, belonging to the 2009 and 2013's R/V OGS Explora surveys in the GT. The average spacing between lines is 1.5 km, while the nearest distance from the eastern and southern coast is about 1.7 km. The distance from the northwestern Friulian Plain coast is about 5 km (Fig. 1).

The 2009 survey collected MCS reflection profiles entirely in Italian waters (Busetti et al., 2010a, 2010b; Zgur et al., 2010).

The 2013 survey, carried out by OGS in collaboration with the University of Ljubljana and Harpha Sea d.o.o. of Koper (Slovenia), acquired MCS profiles that cover the southern part of the gulf, between Italian and Slovenian waters (Busetti et al., 2013; Zgur et al., 2013).

During acquisition of both surveys, the roll-along method was employed. During the 2009 survey, a 600 m long (48 receiver groups) and 1200 m (96 receiver groups) streamer was used for the NW-SE and NE-SW trending profiles, respectively. The 1200 m long digital streamer, with 96 receiver groups, recorded all the 2013 lines. The data acquisition was targeted to recover information with a medium-high resolution (theoretical vertical resolution for shallow layers of about 5 m). Acquisition parameters are listed in Table 1.

The pre-stack data processing in time domain encompassed geometrization, quality control and trace editing, band pass filtering for low and high frequency noise, spherical divergence amplitude correction, predictive deconvolution for reverberation coherent noise removal. Subsequently, after the sorting from shot point (SP) to common depth point (CDP) gathers, the processing involved velocity analyses, normal-moveout correction and stretch mute, stack, post stack deconvolution for multiple removal, automatic gain control, time migration (Zgur et al., 2010, 2013).

4. Methods: traveltime reflection tomography and imaging in depth

The construction of a detailed and reliable seismic velocity field is crucial for an accurate estimation of the spatial distribution of geological elements and can also provide information on underground petrophysical properties.

Seismic reflection tomography represents a versatile tool for the estimation of the interval velocity field and the depth of the interpreted horizons. Compared to the conventional velocity analysis, it allows a better resolution of vertical and lateral velocity variations, which are very important for the better definition of the correct geometries.

In this work we employed two methods to build the velocity-depth model: the Traveltime Reflection Tomography (TRT) and Depth Seismic Imaging (DSI) techniques.

The TRT method (Böhm et al., 1999, 2000; Vesnaver and Böhm, 2000) estimates the velocity field and reflector structure in sequence, from the shallower to the deeper horizon (layer stripping method) by using the following iterative inversion procedure (schematized in Fig. 2a):

Table 1
Acquisition parameters of the 2009 and 2013 seismic campaigns conducted in the Gulf of Trieste, onboard the R/V OGS Explora. Deployed streamer was 600 m long (48 receiver groups) and 1200 m long (96 receiver groups) for the 2009 profiles NW-SE and NE-SW oriented, respectively (Busetti et al., 2010a, 2010b; Zgur et al., 2010, 2013).

Acquisition parameters	2009 SURVEY	2013 SURVEY
Vessel	R/V OGS EXPLORA	R/V OGS EXPLORA
Recording date	October 2009	March 2013
Location	Gulf of Trieste	Gulf of Trieste
SOURCE		
Type	Sleeve guns	GI-gun Sercel
Volume	1180 cu.in.	840 cu.in.
Depth	5 m ± 0.5 m	4 m ± 0.5 m
Shot point interval	12.5 m	12.5 m
Maximum Frequency	150 Hz	187.5 Hz
STREAMER AND RECORDING SYSTEM		
Type	Sercel Seal	Sercel Seal
Length	1200 m/ 600 m	1200 m
Channel number	96/ 48	96
Group interval	12.5 m	12.5 m
Depth	3 m ± 0.5 m	4 m ± 0.5 m
Near offset	25 m	25 m
Maximum fold	48	48
Sampling rate	1 ms	1 ms
Frequency response	flat from 2 Hz to 1 kHz	flat from 2 Hz to 1 kHz
Filters	3 Hz (low cut) – Anti Alias	3 Hz (low cut) – Anti Alias
Record Length	4 s	4 s

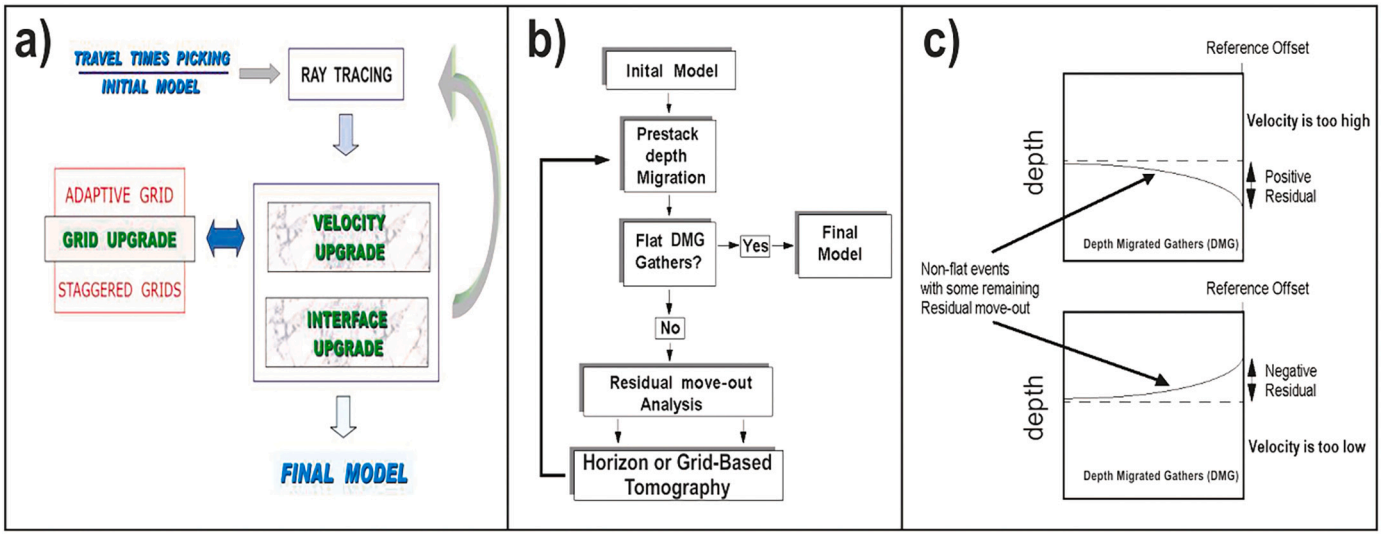

Fig. 2. a) Flow-chart of iterative reflection tomography procedure adopted by the CAT3D (OGS, 2014) software; b) flow-chart of a typical iterative depth imaging procedure and c) residual move out analysis on Depth Migrated Gathers (DMG), adopted by the Paradigm® GeoDepth® software (2017).

1 picking of the traveltimes corresponding to the interpreted horizons for various source-receiver position;
2 definition of an initial model;
3 forward modeling in the initial model, to compute the travel times by performing a ray-tracing for each source-receiver couple. Calculation of the difference between the picked and the modeled travel-times;
4 traveltime inversion, by which the velocity and horizon geometries are upgraded;
5 return to step 3 using the new model, until the difference between this model and the previous one is small enough.

The procedure starts with an initial model for the velocity field and interface structure, generally consisting of homogeneous layers and flat-parallel surfaces. The inversion procedure, performed by the CAT3D software (OGS, 2014), uses the observed travel-times to perform a minimum-time ray tracing. The path between each source and receiver couple is defined through an iterative process following the Fermat's principle (Böhm et al., 1999). The procedure continues for travel-time inversion, by applying the Simultaneous Iterative Reconstruction Technique (SIRT) and computes the seismic velocity through an iterative process that minimizes the travel-time residuals (Stewart, 1991; Van der Sluis and Van der Vorst, 1987). Then, the depth and geometry of the new interfaces are estimated following the principle of minimum dispersion of the reflected/refracted points (Carrion et al., 1993), where the travel-time residuals associated to each reflected/refracted event is converted into depth by using the velocity field updated in the first step of any iteration.

The loop ends when the variations, of the resulting model with respect to that of the previous step, are sufficiently small. This occurs when the dispersion of the estimated reflection points reaches a minimum, so that the reconstructed interface geometry does not vary considerably anymore.

The reliability of the tomographic result can be evaluated by computing the time residuals, that represent the differences between the picked and the computed travel times (Zelt and Smith, 1992). Furthermore, another measure for the reliability of the tomographic inversion is the null space energy, based on the singular value decomposition of the tomographic matrix (e.g. Vesnaver, 1994). This parameter not only depends on the number of rays crossing each pixel, but it is a measure of the linear dependence of the equations associated to the tomographic matrix, and therefore of the matrix rank.

Pre-stack data are generally characterized by seismic signal that is unfocused and exhibits low signal-to-noise ratio. Hence, the detection of primary events at far-offsets can be difficult and relies only on the first traces, especially when the depth of the target exceeds the streamer length adopted for the acquisition. This may result in a rough velocity filed detection and too high dispersion of the estimated depth interfaces. In these difficult cases, pre-stack depth migration is suitable as it focalizes the seismic energy along the reflector, enhancing the signal response and enabling for an easier identification of deeper structures or weak impedance contrasts (Yilmaz, 2001).

Therefore, to further refine the obtained velocity model, we employed the DSI method consisting in an iterative imaging technique involving Pre-Stack Depth Migration (PSDM), residual move-out analysis and tomography (Fig. 2b), by using the Paradigm® GeoDepth® software. Residual move-out analysis uses semblance sections computed vertically or along interpreted horizons on Depth Migrated Gathers (DMG), to assess the remaining error in the velocity field (Fig. 2c). In other words, the degree of non-flatness of the reflection events on the DMG is a measurement of the error in the model (Yilmaz, 2001). Tomography is then performed to refine the velocity-depth model: following the grid- and/or horizon-based approach, it uses residuals as input and attempts to find an alternative model which will minimize the errors in the velocity field and horizon depth to produce flatter gathers (Yilmaz, 2001). Then, the iterative flow proceeds with a new pre-stack depth migration, and it goes on until the residuals become sufficiently small, which means a model with a flat sequence of events (Fig. 2b). In this case, the velocity field is estimated with enough accuracy, allowing to obtain an optimally focused depth image. In our case, the initial model of the refining procedure is that obtained from the tomographic inversion computed by CAT3D software (OGS, 2014). At every iteration both velocity and reflector geometries are updated, until the two sets of parameters reach a good degree of stability and consistency. A new horizon interpretation can eventually be done by picking the migrated section at each iteration. Subsurface imaging is finally obtained by pre-stack depth migration, which uses the refined velocity field to convert the seismic data in an image of the subsurface. The more reliable is the velocity field, the more realistic will be the migrated image.

The time stacked and migrated profiles were also interpreted, by using the IHS Markit® Kingdom® software. The interpreted surfaces were then gridded in the three dimensions by a dedicated algorithm available in the CAT3D software (OGS, 2014).

The final 3D P-wave velocity-depth model of the eastern GT was built throughout a combination of the above described techniques. The detailed workflow steps and related results are described in the following Section 5.

5. Results

The aim of this study was the reconstruction in depth domain of main surfaces and sedimentary units characterizing the sedimentary sequence buried under the Gulf of Trieste, at the northeastern Adria-Eurasia collisional plate boundary. The assessment of their spatial variability and geometrical relationship was done through the integration of different geophysical methodologies (Section 4). The analysis was conducted on several available multichannel seismic reflection lines, located over an area of about 154 km^2 in the eastern part of the Gulf of Trieste.

Starting from the interpretation of the reflected events on time migrated profiles, it was constructed a time 3D time model for the seabed, inner flysch, top flysch, and top carbonates horizons (Section 5.1). Seismic data organized by common shot and offset gathers were also interpreted to obtain, through the TRT method, a reliable 3D P-wave velocity-depth model (A) for the seabed and the top flysch surfaces (Section 5.2).

Since the top of the carbonate could not be picked continuously along the analyzed seismic data, a first 2D tomographic inversion for the top carbonates was performed by using the TRT method (Section 5.3) and the obtained velocity field was then refined by applying the DSI procedure (Section 5.4). This allowed to resolve and image the deeper part of the top carbonates in the eastern study area. Further information came from the refracted event related to the top of the flysch (Section 5.5).

Finally, a 3D P-wave velocity-depth model (B) was constructed by gathering all the information obtained (Section 5.6). The final model bears information about seismic velocities of seawater, Quaternary sediments, upper and lower Eocene flysch, upper Mesozoic-Paleogene Friuli-Dinaric Carbonate Platform together with the depth and geometry of these geological units' top surfaces.

5.1. Traveltimes interpretation and 3D time model

Point 1. of the TRT method consisted in picking the reflected P-wave arrival times related to the seabed and to the top flysch, on pre-stack seismic data sorted by common SP gathers (Fig. 3). The shot gather picking interval represents the number of shot gathers between those gathers on which traveltimes of the main events were observed and detected (picked). This interval was chosen according to the geological structural variabilities detected on common offset or stacked and migrated time sections. Generally, the picking interval was smaller in zones of higher lateral geological variability (e.g., picking interval every 5 shot gathers or less, in correspondence of a steep top carbonates horizon); whereas the interval was larger in correspondence of areas characterized by flat horizons and smoother structures. However, detection of the top carbonates hyperbolas was challenging on part of 2009 data, as the signal is covered by reverberations from shallow seabed (<20 m). The primary events of the top carbonates were detected with higher confidence in 2013 data, on short offsets (maximum 100 m, 4th trace) and at shallower depths than about 0.6 s two-way time (twt). The refracted P-waves arrivals from the top flysch, clearly aligned along a straight event, were also picked on raw pre-stack data. This allowed to directly calculate refraction velocities of the shallower part of the flysch unit (Fig. 4 a,c,e). The resulting horizontal P-wave velocities vary from 3100 and 4200 m/s, with an average value of about 3700 m/s for the entire analyzed dataset. This will be used to obtain average reflection velocities presented in Section 5.5.

The seabed, top flysch and top carbonates, characterized by strong reflection coefficients, were interpreted on the time post-stack migrated data, together with an inner flysch horizon (Fig. 4 b,d). The latter has generally a relative higher amplitude response with respect to that characterizing the upper and lower flysch packages (here named upper and lower flysch, respectively). The resulting 3D time model is shown in Fig. 5. The irregular top flysch surface evidences a general deepening NW-ward and ranges between 0.15 s twt, in the southeastern sector, and 0.3 s twt in the opposite northwestern side. The inner flysch surface ranges between 0.2 and 0.4 s twt and it mimics the above lying top flysch, but it shows more pronounced irregularities. The top carbonates are flexured towards NE, deepening to 0.8 s twt in the easternmost part of the gulf.

5.2. 3D P-wave velocity-depth model A

The first obtained 3D P-wave velocity-depth Model A (Fig. 6) is relative to the top of the flysch and its overburden. The TRT method was applied to invert the reflected traveltimes of the seabed and the top flysch. The initial 3D model was defined by a regular grid made up of 2 horizontal interfaces and 3 homogeneous layers (representing the velocity field). The initial average interval velocities, estimated from the stacking velocities were 1500, 2000, 2500 m/s for water column,

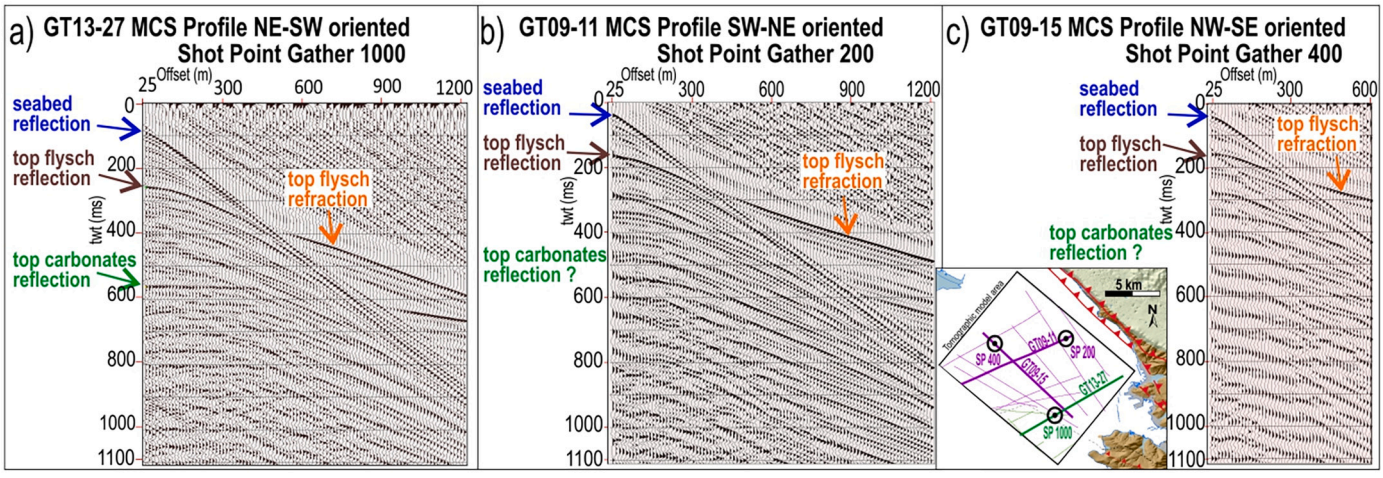

Fig. 3. Pre-stack raw data sorted by common shot gathers of MCS profiles a) GT13–27 (streamer length of 1200 m, 96 channels), b) GT09–11 (streamer length of 1200 m, 96 channels) and c) GT09–15 (streamer length of 600 m, 48 channels). Hyperbolas related to the reflection from the seabed and the top flysch and refraction from top flysch (blue, brown, orange arrows, respectively) can be identified with good certainty. Reflection from the top carbonates (green arrow) is hardly identifiable in 2009 pre-stack raw data, due to reverberations from shallow seabed and high reflection coefficient at top flysch surface. The inset map shows the location of the common shot gathers, displayed in a), b) and c), along their respective seismic profiles. (For interpretation of the references to colour in this figure legend, the reader is referred to the web version of this article.)

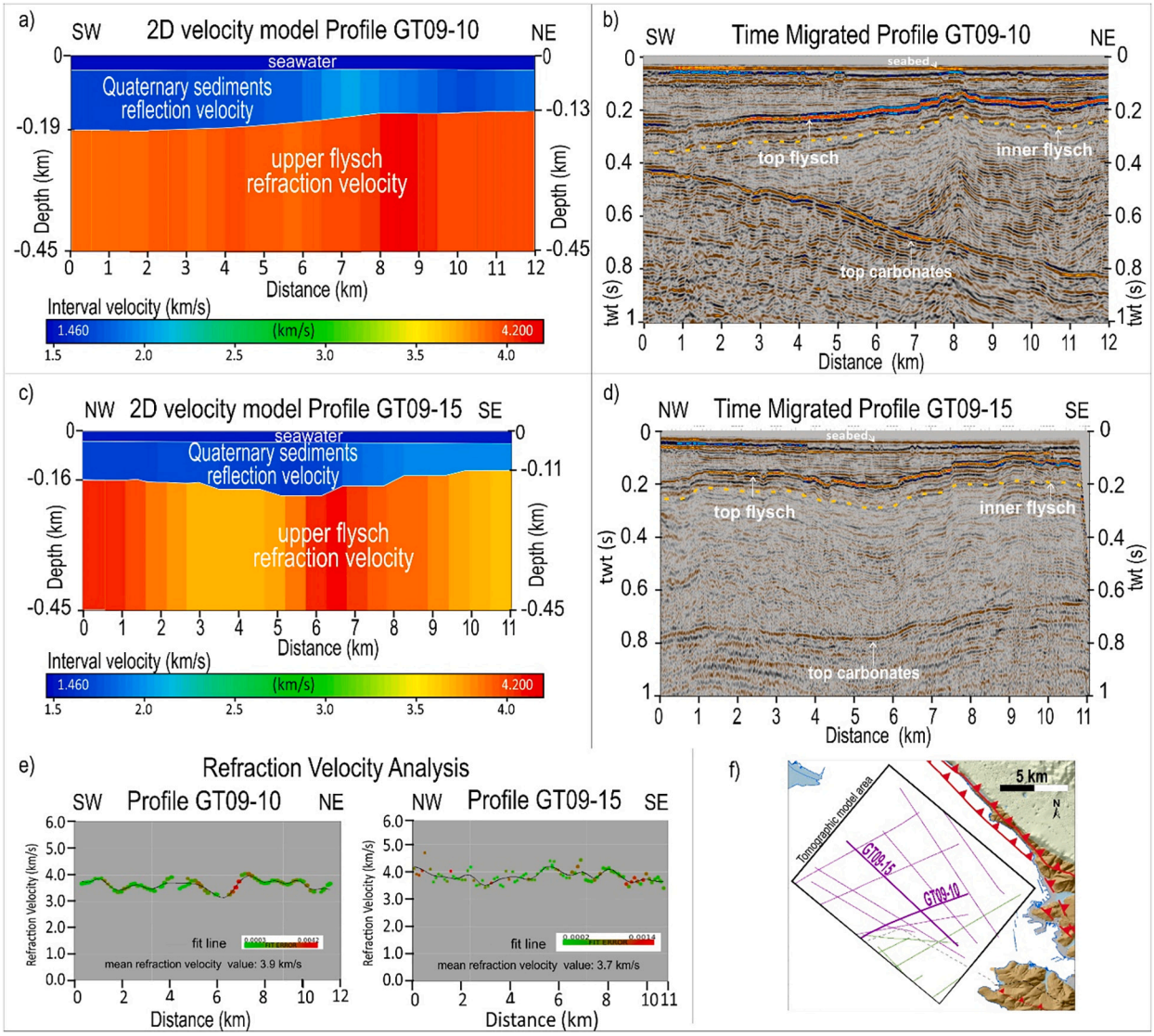

Fig. 4. 2D P-wave velocity depth model for the MCS profiles a) NE-SW oriented GT09–10 and c) NW-SE oriented GT09–15 obtained with CAT3D (OGS, 2014) and represented as time migrated sections in b) and d), respectively. Seabed and top flysch, along with seawater and Quaternary sediments velocities, were reconstructed by means of reflection tomography. The horizontally varying velocity field of the upper flysch unit was estimated by refraction analysis. On the time migrated sections, the seabed, top flysch, inner flysch (dashed yellow line) and top carbonates horizons were interpreted, by using the IHS Markit® Kingdom® software (2014). e) Calculated refraction velocity values for the upper flysch, along the distance of the GT09–10 (left) and GT09–15 (right) profiles, with the best fit interpolation (black line). f) Position map. (For interpretation of the references to colour in this figure legend, the reader is referred to the web version of this article.)

Quaternary sediments and upper flysch, respectively (Picotti et al., 2018). These values are typical velocities for the considered formations (e.g., Schön, 1996; Mavko et al., 2009). Each layer was discretized by a series of 14 voxels along the NW-SE axis and 11 voxels along the NE-SW axis.

After having obtained the velocity of the seawater and the geometry of the seabed, the reflected traveltimes of the top flysch were inverted to define the velocity of the Quaternary sediments and update the top flysch surface geometry. For this latter, the inversion procedure was stopped after 80 iterations, with resulting mean acceptable traveltime residual of 1.5% and 0.003 s. The degree of dispersion of the estimated reflection points in depth, along the top flysch surface exhibits acceptable low values along all the profiles.

The resulting average P-wave velocity of the seawater and underlying layer are 1510 m/s and 1700 m/s, respectively. The estimated depths range is 22–25 m bsl for the seabed and 50–220 m bsl for the top flysch. The former shows an almost flat surface, with highest depths located in the central part of the modeled area. The latter is characterized by irregular morphology, superimposed on a gradual deepening towards NW. The shallowest part of the surface is in the southeasternmost part of the model (along profile GT13–27), about 1.7 km offshore the Trieste coastline.

5.3. 2D P-wave velocity-depth model of the GT13–27 profile

Fig. 7a shows the 2D result of TRT method applied to the eastern part of the GT13–27 (from km 10th to 21st). This is a key profile, as it is almost perpendicular to the northeastern coastline, ending just 1.7 km offshore the city of Trieste. It offers the opportunity to estimate maximum depth of the top carbonates in the footwall of the Karst Thrust. However, the crucial reflection is hardly visible, where it exceeds about 0.6 s twt, in both the analyzed raw pre-stack and stacked data in time domain (Figs. 3a and 7b).

The initial 2D model was constructed similarly to that of Model A, but with a two-dimensional grid (regular) having 3 interfaces and 4 layers. The initial P-wave velocity were (from top to bottom) 1500,

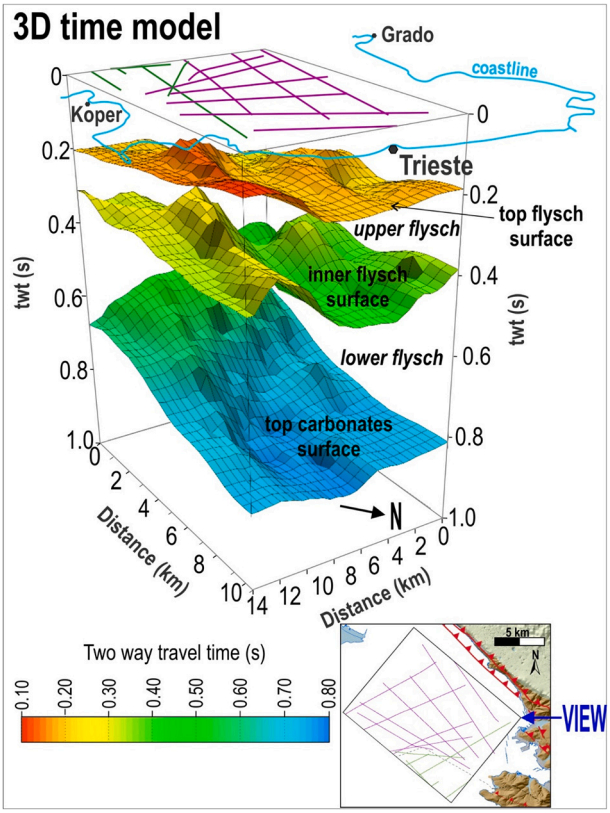

Fig. 5. 3D time model of the investigated area showing twt (s) surfaces of the top flysch, inner flysch and top carbonate, after interpretation of time post-stack migrated data. Gridding (29 × 21 voxels, 483 m × 523 m cell) performed by the OGS CAT3D (OGS, 2014) software, after the interpretation of the horizon on 2D time migrated profiles. The inset map shows the location of the profiles used to produce the 3D time model.

2000, 3500, 4000 m/s. Each layer was discretized by a series of 30 pixels along the SW-NE axis.

Once reconstructed surfaces geometry (seabed, top flysch) and velocities of their overlaying layers, the reflected traveltimes of the top carbonates were inverted to detect the flysch unit velocity and to define the top carbonate depth.

Fig. 7c displays dispersion of the reflection points along the distance of the profile: at shallower depth of the top carbonates, time residuals (Fig. 7d) are acceptable for both short and long offsets (dispersion mean values of about 6 ms). This condition occurs in the southwestern part of the section, where the estimated surface lies between 500 and 800 m bsl. P-wave velocity values for the flysch unit here range between 2800 and 3750 m/s. As the depth of the horizon increases (towards NE), the dispersion of reflected points (picked only up to the 4th trace) increases and the correspondent traveltime residuals reach peaks of 20 ms, indicating that results are not reliable.

5.4. 2D Depth seismic imaging of the GT13–27 profile

To upgrade and refine the P-wave velocity field and geometry, for the different geological units, the DSI method was applied to the analyzed MCS profiles. Despite the typical low reflectivity of inner flysch beds, in this case the reflectivity at the top-mid flysch unit is high enough to apply the velocity refining procedure.

The final PSDM of the GT13–27 profile is shown in Fig. 8. Three iterations were needed to flatten the depth migrated gathers and therefore to obtain an optimal focused seismic imaging, also for the inner flysch beds.

Well defined P-wave velocity vertical gradients are detected for main sedimentary units: 1600 to 2100 m/s for the Quaternary sediments, 2900 to 4500 m/s for the Eocene flysch unit, and 4600 to 5300 m/s for the FDCP.

Considering the profile of Fig. 8a, the top FDCP dips gradually northeastward, with a mean real angle of 5° along the profile direction (N60°E). The horizon reaches a maximum depth of 1600 m ± 50 m bsl, in the easternmost gulf. The error is estimated by considering an amplitude coherence of 70%, although seismic vertical theoretical resolution at that depth is about 30 m. The flysch unit shows maximum thickness of about 1500 m (top surface at 100 m bsl), that gradually decreases SW-ward. Erosive truncations are clearly visible at the top surface, that is overall depicted by irregular shape. At km 7 and depth of 200 m bsl, the flysch closes against the top of the carbonates and has subverticalized layers concordant with the top carbonates surface.

At 4.8 km depth, in correspondence of DMG 455, the average interval velocity reaches 4800 m/s and a quite well focused reflection is highlighted (Fig. 8b).

Seismically, it is characterized by a strong amplitude and reverse polarity. We exclude that this event can be associated to the multiple reflection of the top carbonates, because it occurs at a two-way time value (about 2 s twt) that is much larger than the double of that of the top carbonates (about 1.5 s twt, in correspondence of DMG 455 on the GT13–27 profile). Whereas, the reverse polarity is related to a velocity inversion. This is validated by the stratigraphy and sonic log of the Amanda 1bis well (Nicolich et al., 2004; ViDEPI-Project, 2009; Patricelli and Poli, 2020), located in the central part of the northern Adriatic, some tens of kilometers W from the presented GT13–27 profile and reaching 7305 m depth. The well crosses the basinal Meso-Cenozoic carbonate sequence (thus it does not intersect the FDCP carbonate units occurring in the GT). The sonic log carried out in this well shows a velocity drop of about 1000 m/s at a depth of about 5300 m, according to the reversed polarity of the reflected event in our data. Although it is a well-known seismostratigraphic horizon extending through the north Adriatic and Venetian Friulian Plain (e.g., Nicolich et al., 2004; Zanferrari et al., 2008), this deep and strong reflected event is well detectable only in some local areas on the analyzed profiles. The seismic discontinuity is due to the fact that the event sits at a depth that is much larger than the maximum offset of the multichannel profile. This hampers the move-out sensitivity for the accurate reconstruction of the velocity field in the deeper formations. Moreover, the event occurs below an almost flat top carbonate surface (as in the correspondence of DMG 455 of the GT13–27 profile), in correspondence of which the incident rays are little deflected and the seismic energy is better focused. The same regards the seismic tomography which cannot estimate horizons at much higher depth with respect to the maximum offset. The velocity inversion is related to the change in the stratigraphic sequence: from the upper Triassic - Paleogene Carbonates to a 700 m thick upper Triassic package rocks of dolostones intercalated by pelitic layers locally rich in organic matter (Monticello Fromation), alternation of sands, marls and clays, evaporites (Trevenanzes Formation), dolostones (Dolomia Cassiana), hyaloclastites (Wengen Formation) and basic lavas (Vulcaniti), underlain in turn by a Permo - middle Triassic Carbonate sequence (Nicolich et al., 2004).

5.5. 2D P-wave velocity-depth models from top flysch refraction

The horizontally varying velocity field of the upper flysch unit was estimated by refraction analysis (Fig. 4 a,c,e), described in Section 5.1.

The analysis, performed on all the seismic profiles, evidences a marked discrepancy between the average reflection (almost vertical) and refraction (almost horizontal) velocities at the upper flysch layer, which are about 2900 m/s and 3700 m/s, respectively.

This large discrepancy can be interpreted as a pronounced anisotropic effect, due to the laminated internal structure of the flysch unit. Most geological systems can be modeled as fine layering at seismic frequencies, which occurs when the dominant wavelength of the pulse is

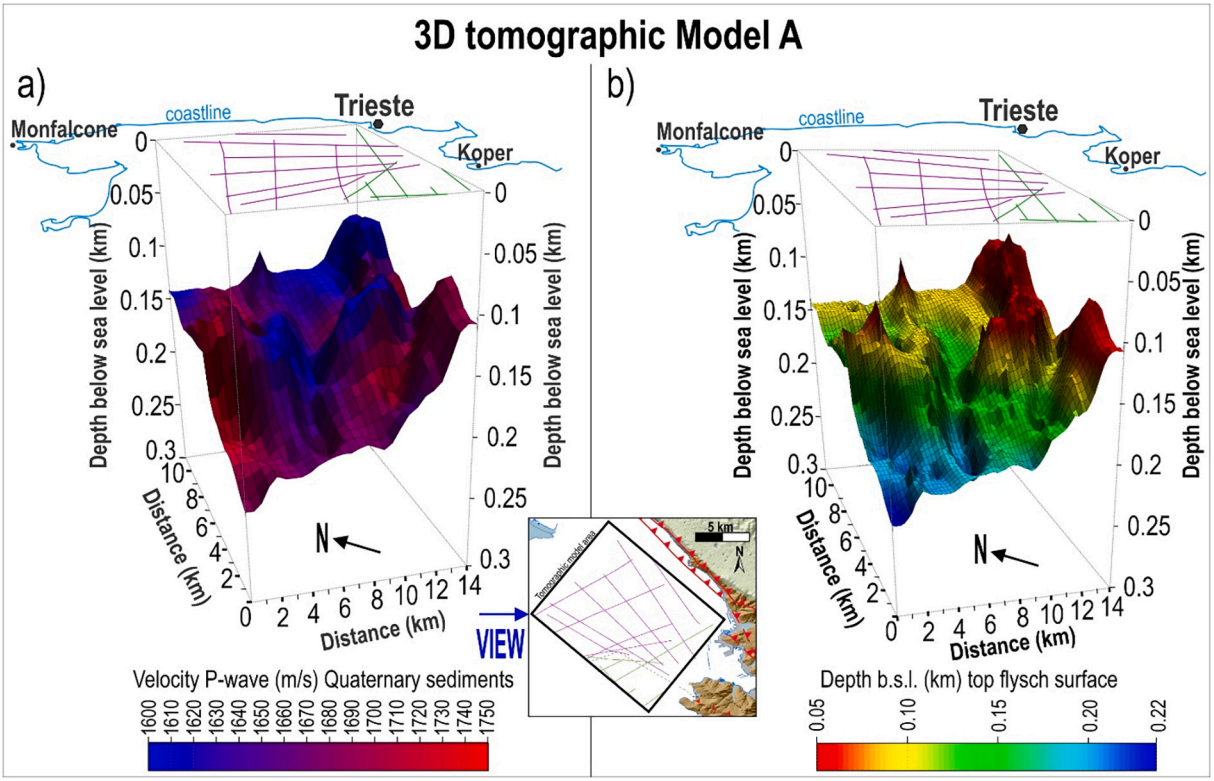

Fig. 6. Model A. Results of TRT performed by using CAT3D (OGS, 2014): a) 3D P-wave velocity depth model of the top flysch surface. The Quaternary sediments have an average velocity of 1720 m/ s. b) 3D depth model of the top flysch surface, characterized by irregular morphology with minimum and maximum depths of 50 m and 220 m, respectively. The inset map shows the location of the profiles used to produce the 3D P-wave velocity-depth model A.

much larger than the thicknesses of the single layers. Picotti et al. (2018) validated the large discrepancy between the two tomographic velocity values by considering the flysch composed of a thin-layer periodic sequence of loose shale and cemented sandstone, and by applying the averaging theory by Backus (1962). Because of the inner flysch beds are almost horizontal, except for some locally tectonized sectors, the anisotropic model has a symmetry axis which is almost vertical, and the medium can be considered VTI (i.e., Vertical Transverse Isotropic; Picotti et al., 2018).

In other words, the difference between the average reflection and refraction velocities at the upper flysch layer, in the study area, can be interpreted as the anisotropic effect due to the laminated internal structure of the flysch unit.

5.6. 3D P-wave velocity-depth model B

The final 3D P-wave velocity-depth Model B (Fig. 9) was built by combining the below listed outcomes:

a) average P-wave velocity of about 1510 m/s and 1700 m/s for the seawater and for the Quaternary sediments, respectively. Both belonging to Model A, obtained by the TRT technique, providing also the seabed and top flysch depth geometries;

b) P-wave vertical velocity ranging between about 2800 and 3100 m/s for the upper flysch unit, calculated from the horizontally varying refraction P-wave velocity by using the flysch anisotropic coefficients obtained by Picotti et al. (2018). These velocities are therefore used to convert into depth the inner flysch surface of 3D time model;

c) average P-wave velocity of 4500 m/s for the lower flysch unit, obtained from the DSI method performed on the GT13–27 profile. This average P-wave velocity is therefore used to convert into depth the top carbonates surface of the 3D time model.

The Model B shows the general NE-ward deepening of the top FDCP. Its depth ranges between 1450 and 1550 m bsl, along the northeastern side of the model, close to the coast. It gradually rises to 1000 m and 800 m in the northwestern and southwestern edges of the model, respectively. The surface shows a pattern of high and low morphologies, whose longitudinal axis is NW-SE oriented.

The top carbonates, interpreted along the PSDM GT13–27 profile, is shown within the Model B (yellow line in Fig. 9). There is a good degree of approximation (considering the large depth of this surface), except from some local discrepancies (up to ±90 m), as those in correspondence of the northeastern most part of the PSDM profile, where the local difference is about ±75 m. These differences are due to the fact that the 2D interval velocity model of the GT13–27 profile was refined using the iterative depth imaging procedure described in Section 4 and Fig. 2b.

6. Discussion

Considering the resulting depth models, the thickness of the marine and continental Quaternary sediments, characterized by well-organized reflective packages, reaches a minimum in the eastern part, while they increase towards W-NW, in accordance with Busetti et al. (2010a, 2010b). Thickness values range from a minimum of about 50 m in the eastern part of gulf and a maximum of 190 m in the opposite side within the analyzed volume.

The DMG455 analyzed by the DSI procedure, together with the adjacent gathers within a 2 km segment of the PSDM section (Fig. 8b), shows a strong 4.8 km deep event, representing the base of the upper Triassic - Paleogene carbonate sequence (in the GT comprising the Dolomia Principale and the FDCP units, see also Section 5.4). It can be estimated that the thickness of the sequence, at least in the southeastern gulf, is around 3200–3400 m. This strong and deep event is a well-known seismostratigraphic horizon occurring at a basin-scale in the north Adriatic and Venetian Friulian Plain (e.g., Nicolich et al., 2004; Patricelli and Poli, 2020; Zanferrari et al., 2008). Since this reflection represents a seismically discontinuous horizon along the analyzed

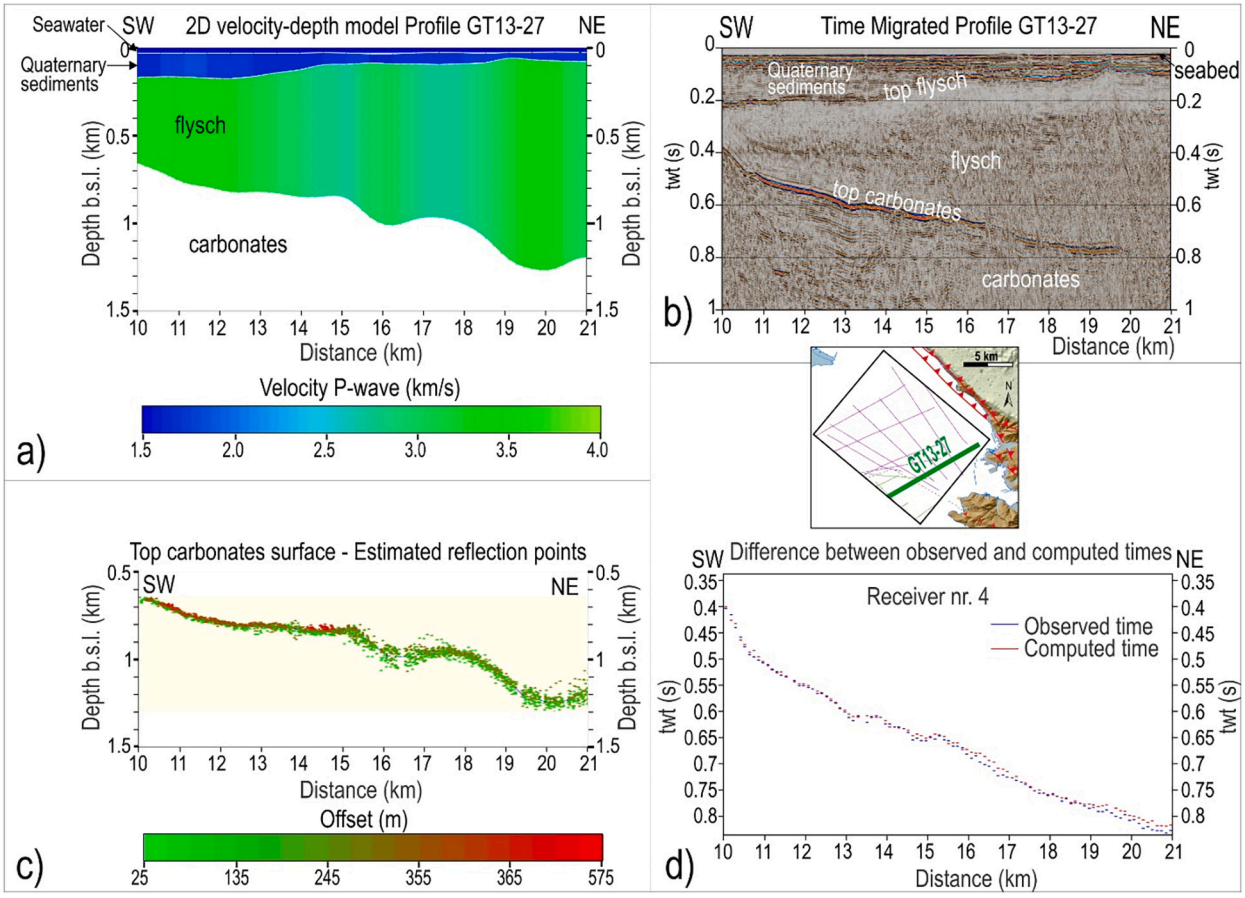

Fig. 7. a) 2D P-wave velocity depth model for the northeastern MCS profile GT13–27, NE-SW oriented, performed by CAT3D (OGS, 2014). b) time stacked MCS profile GT13–27 c) Plot of estimated reflection points (red and green refer to longer and shorter offsets, respectively) for top carbonates surface estimation along the distance of the profile. d) Plot of the observed and computed travel times (for the 4th traces, 100 m offset) for top carbonates surface estimation, along the distance of profile and position map. The inset map shows the location of the analyzed seismic profile. (For interpretation of the references to colour in this figure legend, the reader is referred to the web version of this article.)

profiles, it could not be modeled and presented in the final 3D model. Therefore, the estimated thickness of the upper Triassic - Paleogene carbonate sequence represents a local value, but in agreement with the Amanda 1bis well stratigraphy. This event is locally evident also in other parts of the profiles and this demonstrates the good compromise between resolution and penetration provided by the analyzed MCS reflection lines.

Fig. 10 integrates the results with the onland geology known from literature, combining different structural domains separated by the Karst Thrust (Dinaric foredeep to the W and External Dinarides to the E). The flysch reaches its maximum thickness of about 1500 m in the eastern side of the tomographic model, where it fills the Dinaric foredeep in the footwall of the thrust. The unit thins towards W where it is about 600 m thick. Further W, it pinches out on the top carbonate surface. The top flysch surface deepens from 50 m to 220 m depth bsl NW-ward. The depth imaging profile shows that the upper part of the flysch is characterized by internal layering that bends upwards from sub-horizontal to sub-vertical dip westward. This configuration can be interpreted as the effect of compressive deformation SW-ward verging, during the final stages of the Dinaric tectonic phase occurring in the Paleogene. The upper flysch unit results to be about 250 m thick. Its base is represented by the inner flysch surface that, with respect to the top flysch surface, is more uneven. This may reflect different intensities of tectonic deformation, as suggested by Busetti et al. (2010a, 2010b).

The top of the Meso-Cenozoic FDCP, buried in the gulf, deepens gradually towards NE and it is characterized by smooth ridges and valleys SW-NE elongated and few meters wide. The different style of deformation between the two units reflects their rheological contrast: ductile for the turbiditic flysch and rigid for the tilted carbonate bedrock.

At about 1.7 km from the Trieste coast, the top FDCP reaches a maximum depth of 1600 ± 50 m below sea level (bsl). The resulting depth in Model B fits, with a good degree of approximation, the depth revealed by the PSDM (maximum misfit: ± 90 m). Local discrepancies (Fig. 9) are anyhow due to the interval velocity function, detected by the PSDM within the flysch unit, that is vertically and horizontally detailed with higher accuracy through DMG residual analysis, while in the 3D model the lower flysch unit has constant velocity. An example related to this difference can be seen near to the Trieste coast: here the top carbonates surface reaches a depth 1550 m bsl in the 3D surface of model B, while it is about 75 m deeper according to the PSDM result.

In the footwall of the Karst Thrust system, the depth of the top FDCP can be extrapolated, using the average inclination of 5°, down to 1740 m bsl in correspondence of the Trieste shoreline. The Karst Thrust system, NW-SE oriented and SW vergent, extends along the rocky coast and continues southeastward as the Črni Kal (in Istria) and northwestward as the Panzano Thrust (in the northern gulf and southeastern Friulian Plain). Moreover, at sea, the Sistiana left transtensive fault offsets the tectonic lineament few kilometers westward (Fig. 10a).

Along the shoreline and in the correspondent hinterland Karst Plateau, the Mesozoic-Paleogene lithostratigraphic units are structured in a Dinaric anticline (NW-SE axis) elevating between 0 and about 600 m asl on the eroded topographic surface (with a general lowering trend NW-wards). This represents the hanging-wall of the Karst Thrust, that

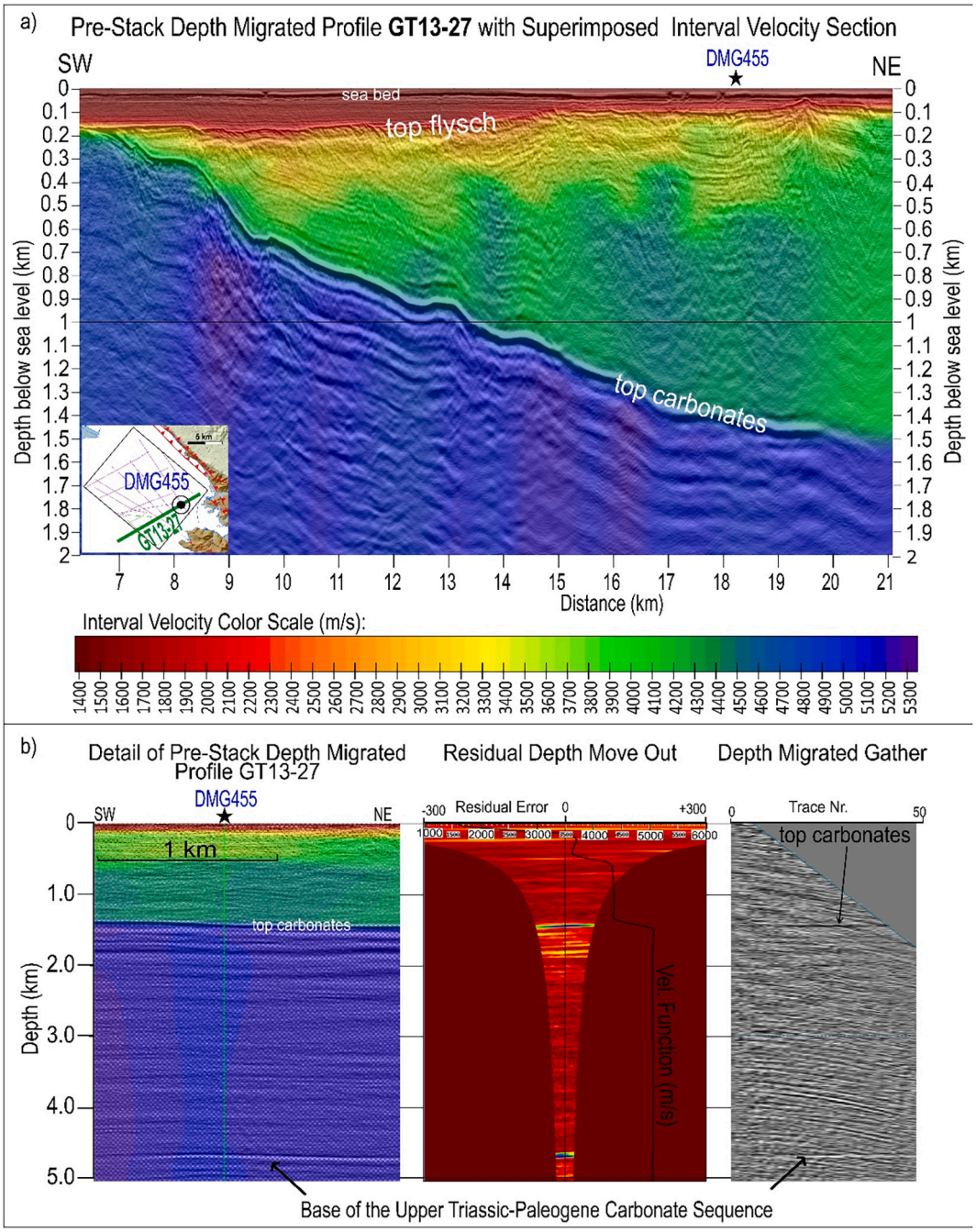

Fig. 8. Result of the depth seismic imaging procedure (Pre-Stack Depth Migration, PSDM, vertical exaggeration about x4) on the GT13–27 profile, with superimposed the refined P-wave velocity field. The top carbonates surface reaches a depth of 1600 m below sea level, 1.7 km far from the coast of the city of Trieste. The black star indicates position of the depth image gather (DMG) nr. 455 represented in detail in b) where, from left to right are shown: detail of the PSDM up to a depth of 5 km (the base of the Upper Triassic-Paleogene carbonate reflection is highlighted), with superimposed interval velocity section, the residual moveout panel with velocity function (black line) and the corresponding flat sequence of reflected events of the DMG. In this DMG, the hyperbolic events which have not been flattened correspond to multiples of the base flysch-top carbonates interface. The flattening of these events leads to much lower velocities values than those of the geological unit (carbonates) at that depth. Performed by using Paradigm® Geodepth® (2017) software. The inset map shows the location of the analyzed DMG and seismic profile.

brings the carbonate units above the younger Eocene flysch (structured, towards the coastline, in almost vertical dipping layers). The geological profile of Fig. 10d represents this structural setting. It was reconstructed along the SW-NE pre-stack depth migrated GT13–27 profile and its imaginary linear prosecution across the entire Karst Plateau up to the Vipava Fault. The onshore section is built by using jointly the geological maps published by GEO-CGT (2013) and Jurkovšek et al. (2016). The GEO-CGT (2013) covers the Classical Karst geology for the Italian territory, while the Slovenian part of the Karst is covered by the geological map by Jurkovšek et al. (2016). No wells are available in the area. Moreover, the depth extensions of the Divača, Tomačevica and Raša faults are reported from analyses of the seismicity in the area by Guidarelli et al. (2017) and Vičič et al. (2019). Despite the fault plane of the Karst Thrust is not imaged by seismic data, we can assume a geometry similar to the thrust system buried below the Friulian Plain and imaged by exploration seismic profiles (e.g., Merlini et al., 2002;

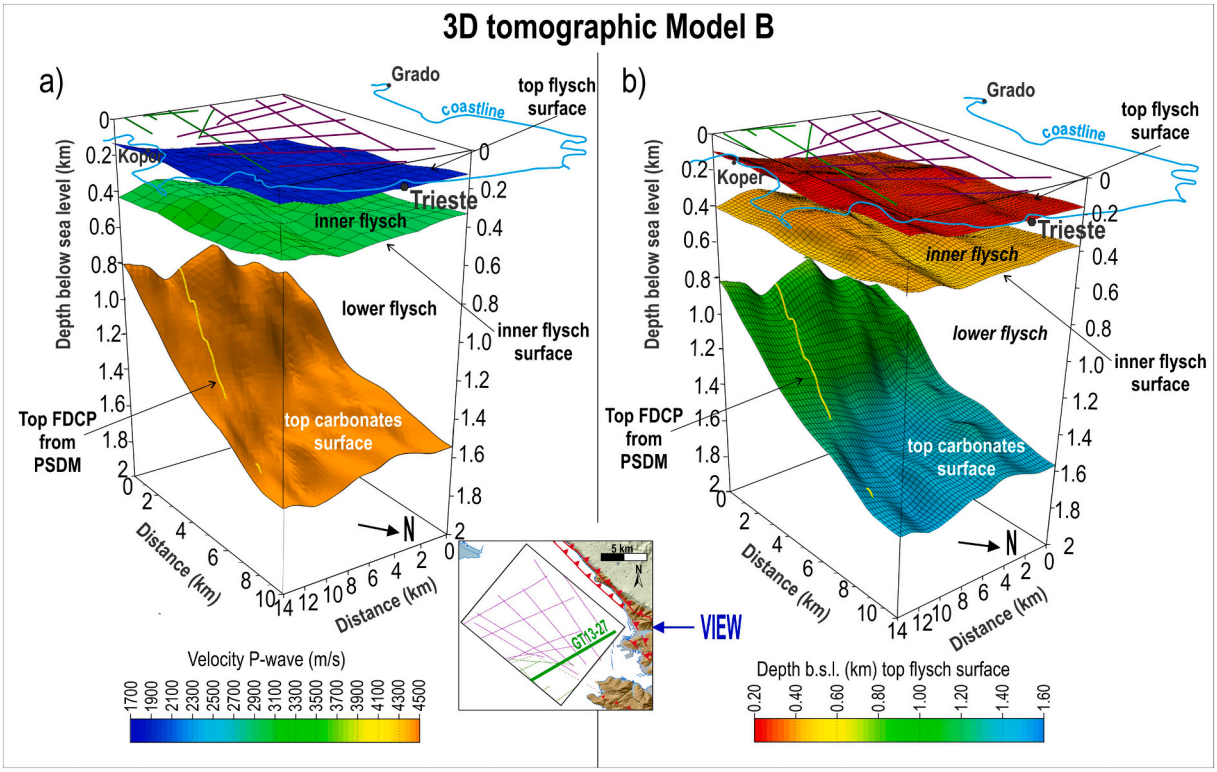

Fig. 9. Hybrid Model B, that is the final results from the applied tomographic techniques: a) 3D velocity depth model of main units in the eastern GT. The Quaternary sediments, the upper flysch, the lower flysch and the carbonates have an average P-wave velocity of 1720 m/s, 3100 m/s, 4500 m/s, respectively. b) 3D depth model, built using the CAT3D (OGS, 2014) software, of (from top to bottom): the top flysch, inner flysch and top carbonates depth surfaces. The yellow line, along the top FDCP, represents the top carbonates picked horizon along the PSDM of GT13–27 profile. The inset map shows the location of the profiles used to produce the 3D P-wave velocity-depth model B and the GT13–27 profile on which the yellow line of the top carbonates horizon was interpreted. (For interpretation of the references to colour in this figure legend, the reader is referred to the web version of this article.)

Nicolich et al., 2004) and constituting the system to which the Karst Thrust belongs. Assuming the tectonic style of the buried thrusts, the Karst Thrust is considered to significantly displacing the FDCP. The top carbonate cut off at the hanging wall could be estimated to be around 100 m asl (Fig. 10d). Based on these evidences, the vertical throw, in correspondence of the coast, given by the Karst Thrust could be estimated in about 1800 m. Fig. 11 shows the three-dimensional geological setting over the surrounding onshore of the gulf (from 3D depth model B), where the Karst highland and southeastern Friulian Plain (Digital Elevation Model by IRDAT, 2017) are represented together with outcropping faults and lithologies (from the geological maps by GEOCGT, 2013; Jurkovšek et al., 2016). Whereas, in adjacent marine foredeep (eastern gulf), the top flysch and top FDCP depth surfaces are represented and gridded from the MCS pre-stack depth migrated profiles processed in this work. Fig. 11 is part of the 3D video multimedia uploaded as Supplementary data to this article.

7. Conclusion

This study provides the first well-constrained 3D elastic P-wave velocity and depth model of the sedimentary sequence in the submarine Dinaric foredeep, adjacent to the northeastern collisional boundary between Adria and Eurasia. This was done by applying and integrating different advanced tomographic techniques on a recently acquired MCS reflection dataset, located over an area of 154 km^2 in the eastern GT. The combined traveltime reflection tomography and depth seismic imaging procedures yielded detailed seismic velocities for the Quaternary sediments, Eocene turbiditic flysch and Meso-Cenozoic Friuli Dinaric Platform Carbonates. Therefore, depth and geometries of top flysch, inner flysch and top carbonates surfaces are quantitatively assessed in the foredeep of the External Dinarides. The resulting P-wave velocity field provides mean values of 1510 m/s for the seawater, 1700 m/s for the Quaternary sediments, 2900 m/s for the upper flysch, 4500 m/s for the lower flysch, 5000 m/s for the carbonates. The outcomes reveal that the top of the Meso-Cenozoic carbonates is an inclined plane that reaches a maximum depth of 1600 ± 50 m bsl, about 1.7 km offshore the city of Trieste. If linearly extrapolated in correspondence to the shore, the horizon depth reaches about 1740 m bsl. Considering the Karst Plateau elevating up to 600 m asl, and the possible top carbonate cut off at the hanging wall at about 100 m asl, the Karst Thrust is responsible for a vertical throw of about 1800 m, in correspondence to the Trieste coast. Moreover, the 3D velocity-depth model and the depth imaging reveal that the maximum thickness of the flysch unit, filling the External Dinaric foredeep at the footwall of the Karst Thrust, is about 1500 m. The Gulf of Trieste is yet devoid of major known earthquakes in the historical and instrumental periods, but it is embedded over a deformed continental margin, where neotectonic activity is proven by a wealth of geophysical and geomorphic data and it is due to the active NNW-ward motion of Adria microplate. Therefore, these new quantitative outcomes offer enhanced constraints for neotectonic evaluation in this highly urbanized and industrial area. Resulting velocities of main units represent reference values for advanced seismic processing and data analysis to reconstruct buried geometries under the southeastern Friulian Plain, where geological setting is analogous, being the Panzano Thrust considered the northwestward continuation of the Karst Thrust. Moreover, the accurately reconstructed depth geometries of main sedimentary units, in the External Dinarides foredeep and Southeastern Alps foreland, provide new insights into the Adria lithospheric processes, that are prominent players within the Mediterranean geodynamics.

Supplementary data to this article can be found online at https://doi.

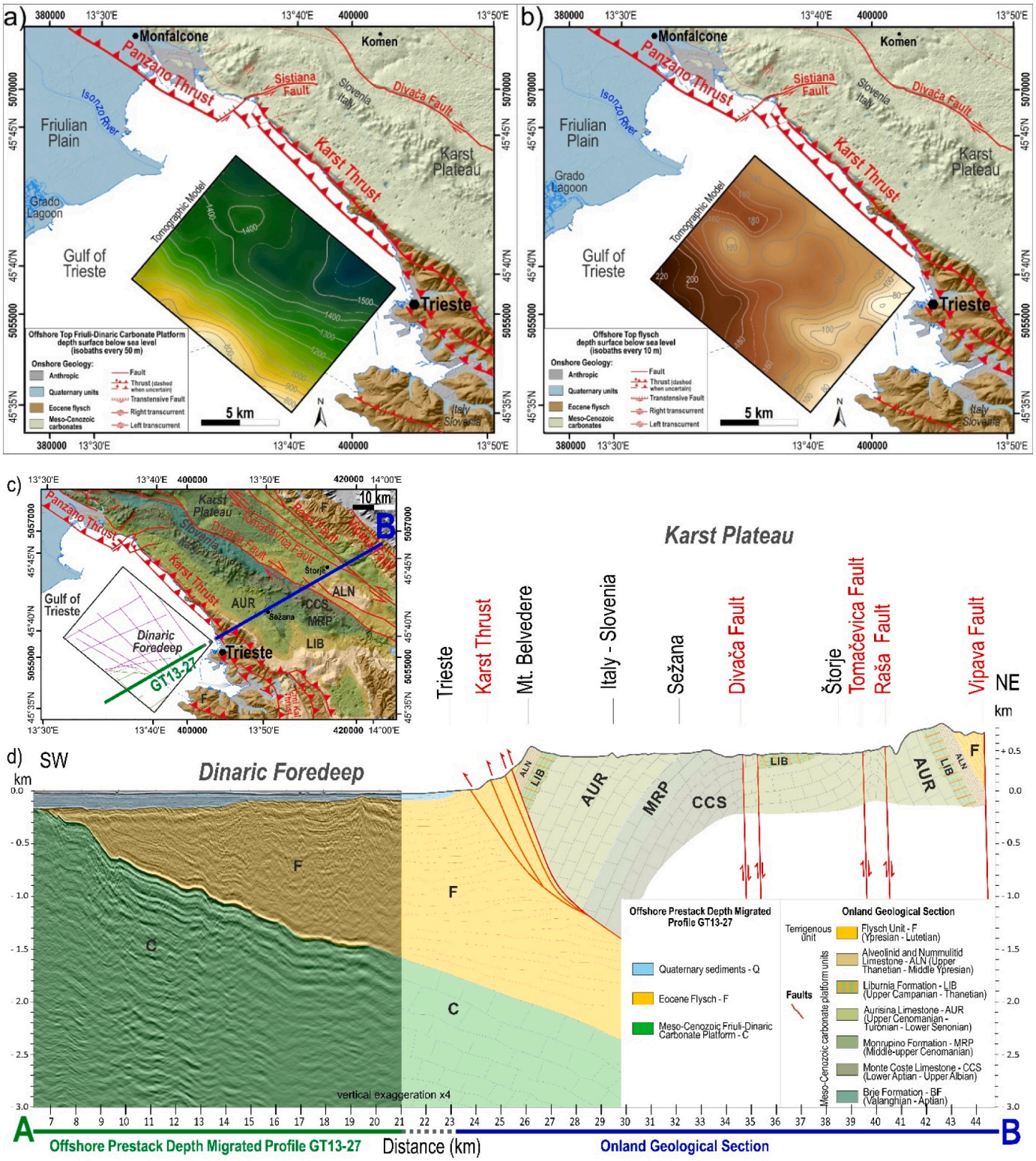

Fig. 10. Integration of geophysical results with surrounding geology. Maps of a) the top carbonates and b) the top flysch depth surfaces, obtained from the 3D depth model B, within the eastern side of the Gulf of Trieste. Offshore depths are represented by the graded colour scales (contours every 50 m and 10 m, respectively). c) Geological map with location of the cross section shown in d). d) Offshore-onland geological section crossing the Dinaric foredeep in the gulf and the entire Karst Plateau along SW-NE direction. Composed by the PSDM result for the GT13–27 profile and adjacent classical geological section reconstructed from onland geological information (GEO-CGT, 2013; Jurkovšek et al., 2016). The top of the carbonates reaches the depth of 1.6 km at the NE end of the GT13–27 profile, and it is estimated to reach about 1740 m bsl under the city of Trieste. The carbonate units outcrop on the Karst anticline up to an elevation of 600 m asl, with the cutoff at the hanging wall at around 100 m. As consequence, the vertical throw related to the Karst Thrust, in correspondence of the coast, could be estimated to be about 1.8 km. Maps compiled by using ESRI® ArcGis® (2016) software; datum WGS84, projection UTM33.

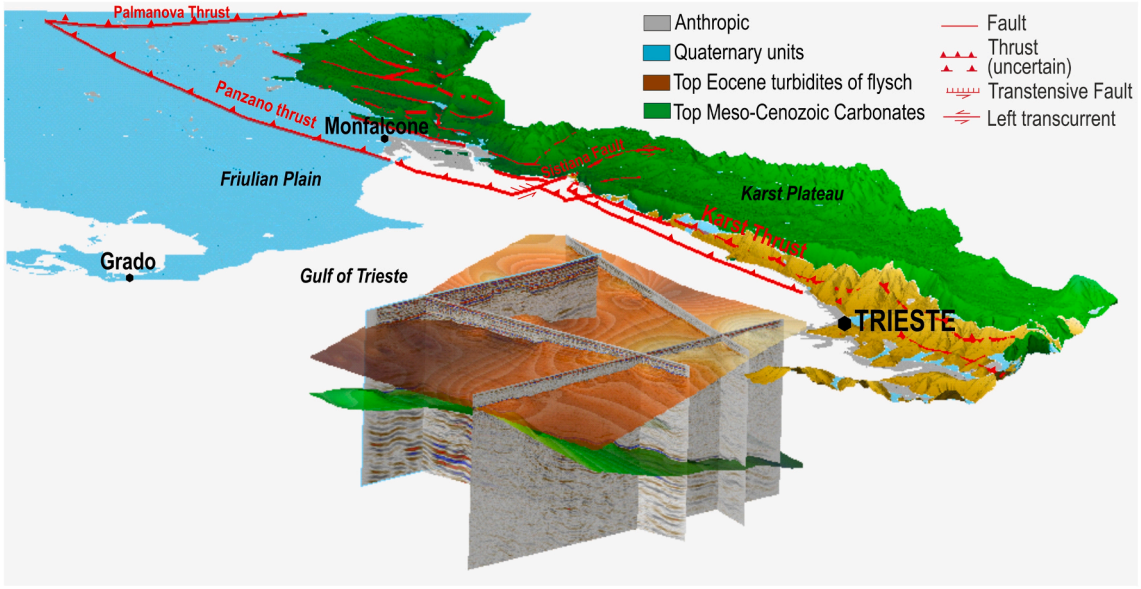

Fig. 11. Three-dimensional geological model (view from SW) representing the main marine surfaces reconstructed inside the External Dinarides foredeep (3D depth Model B), together with the adjacent onshore geological model (from GEO-CGT, 2013; Jurkovšek et al., 2016) draped over an elevation map. The Karst highland and southeastern Friulian Plain (Digital Elevation Model by IRDAT, 2017) are represented together with outcropping faults and lithologies. In the eastern gulf, the top flysch and top FDCP depth surfaces are shown together with some of the resulting MCS pre-stack depth migrated profiles processed in this work. Vertical exaggeration: x4. This figure is part of the 3D video multimedia uploaded as Supplementary data to this article. 3D model compiled by using the Schlumberger® Petrel® software.

org/10.1016/j.tecto.2022.229470.

Funding

This research was the main subject of the first author's PhD course at the University of Trieste. The work was developed at the National Institute of Oceanography and Applied Geophysics – OGS, in the frame of the first author's PhD granted by the Commissariato del Governo nella Regione Friuli Venezia Giulia (Italy), through the "Fondo Trieste" fund.

Data availability

Data is available through Busetti et al. (2010a, 2010b, 2013), Dal Cin (2018), Picotti et al. (2018).

CRediT authorship contribution statement

Michela Dal Cin: Conceptualization, Data curation, Methodology, Formal analysis, Validation, Writing – original draft, Writing – review & editing, Visualization. **Gualtiero Böhm:** Conceptualization, Data curation, Methodology, Software, Validation, Resources, Writing – review & editing, Supervision. **Martina Busetti:** Conceptualization, Methodology, Validation, Investigation, Data curation, Resources, Writing – review & editing, Supervision, Project administration, Funding acquisition. **Stefano Picotti:** Methodology, Software, Validation, Resources, Data curation, Writing – review & editing, Supervision. **Fabrizio Zgur:** Methodology, Software, Validation, Investigation, Data curation, Writing – review & editing, Supervision. **Angelo Camerlenghi:** Conceptualization, Resources, Writing – review & editing, Supervision, Funding acquisition.

Declaration of Competing Interest

The authors declare that they have no known competing financial interests or personal relationships that could have appeared to influence the work reported in this paper.

Acknowledgments

The authors acknowledge IHS Markit®, Paradigm® and Schlumberger®, that provided the academic Kingdom®, GeoDepth®, Vista® software licenses to OGS and Petrel® license to the University of Trieste. We thank the anonymous reviewers, whose constructive comments allowed to improve the manuscript.

References

Accaino, F., Busetti, M., Böhm, G., Baradello, L., Affatato, A., Dal Cin, M., Nieto, D., 2019. Geophysical investigation of the Isonzo Plain (NE Italy): imaging of the Dinaric foredeep at the Alpine-Dinaric chain convergence zone. Ital. J. Geosci. 138, 202–215. https://doi.org/10.3301/IJG.2019.01.

Arso, 2017. Ministry of the Environment and Spatial Planning. Slovenian environment agency. Available at: https://gis.arso.gov.si.

Backus, G.E., 1962. Long-wave elastic anisotropy produced by horizontal layering. J. Geophys. Res. 67, 4427–4440.

Böhm, G., Rossi, G., Vesnaver, A., 1999. Minimum-time ray-tracing for 3-D irregular grids. J. Seism. Explor. 8, 117–131.

Böhm, G., Galuppo, P., Vesnaver, A., 2000. 3-D adaptive tomography using Delaunay triangles and Voronoi polygons. Geophys. Prospect. 48 (4), 723–744.

Braitenberg, C., Romeo, G., Taccetti, Q., Nagy, I., 2006. The very broad-band data acquisition of the long-base tiltmeters of Grotta Gigante (Trieste, Italy): secular term tilting and the great Sumatra-Andaman Islands earthquake of December 26, 2004. J. Geodyn. 41, 164–174.

Brancolini, G., Civile, D., Donda, F., Tosi, L., Zecchin, M., Volpi, V., Rossi, G., Sandron, D., Ferrante, G.M., Forlin, E., 2019. New insights on the Adria plate geodynamics from the northern Adriatic perspective. Mar. Pet. Geol. 109, 687–697. https://doi.org/10.1016/j.marpetgeo.2019.06.049.

Burrato, P., Poli, M.E., Vannoli, P., Zanferrari, A., Basili, R., Galadini, F., 2008. Sources of Mw 5+ earthquakes in northeastern Italy and western Slovenia: an updated view based on geological and seismological evidence. Tectonophysics 453, 157–176.

Busetti, M., Volpi, V., Nicolich, R., Barison, E., Romeo, R., Baradello, L., Ramella, R., 2010a. Dinaric tectonic features in the Gulf of Trieste (Northern Adriatic). In: D. Slejko (Ed.), Novelties in Geophysics, Select paper from the 27th Annual Conference of the Italian Group for Solid Earth Geophysics, Trieste. Boll. Geofis. Teor. Appl. 51 (2–3), 117–128.

Busetti, M., Volpi, V., Barison, E., Giustiniani, M., Marchi, M., Ramella, R., Zanolla, C., 2010b. Cenozoic seismic stratigraphy and tectonic evolution of the Gulf of Trieste (Northern Adriatic). Proceedings of the "ADRIA 2006 – International Geological Congress on Adriatic area". GeoActa SP3, 1–14.

Busetti, M., Zgur, F., Vrabec, M., Facchin, L., Pelos, C., Romeo, R., Zerial, A., 2013. Neotectonic reactivation of Meso-Cenozoic structures in the Gulf of Trieste and its relationship with fluid seepings. Proceedings of the 32nd Gruppo Nazionale di

Geofisica della Terra Solida (GNGTS) Congress, Trieste 19–21 November 2013. 3-Appl. Geophys. 29–34.
Busetti, M., Babich, A., Del Ben, A., 2019. Geophysical evidence of fluids emission in the Gulf of Trieste (North Adriatic Sea). Mem. Descr. Carta Geologica d'Italia 105, 11–16.
Carminati, E., Doglioni, C., 2012. Alps vs. Apennines: the paradigm of a tectonically asymmetric Earth. Earth Sci. Rev. 112, 67–96.
Carrion, P., Böhm, G., Marchetti, A., Pettenati, F., Vesnaver, A., 1993. Reconstruction of lateral gradients from reflection tomography. J. Seism. Explor. 2, 55–67.
Castellarin, A., Nicolich, R., Fantoni, R., Cantelli, L., Sella, M., Selli, L., 2006. Structure of the lithosphere beneath the Eastern Alps (southern sector of the TRANSALP transect). Tectonophysics 414, 259–282.
Cati, A., Sartorio, D., Venturini, S., 1987. Carbonate Platforms in the Subsurface of the Northern Adriatic Area. Mem. Soc. Geol. It. 295–308.
Dal Cin, M., 2018. 3D velocity depth model in the Gulf of Trieste by means of tomographic analysis from multichannel seismic reflection data. PhD thesis, course Earth Science and Fluid Mechanics. University of Trieste, OGS and ICTP, Trieste, March 2018, 212 pp. Supervisor: A. Camerlenghi; co-tutors: M. Busetti, G. Böhm, S. Picotti and F. Zgur. http://hdl.handle.net/11368/2922569.
Della Vedova, B., Cimolino, A., Castelli, E., Brancatelli, G., 2014. Geothermal Heating and Cooling in the FVG Region: the Grado District Heating and the Pontebba Ice Rink Plants. Status and future in the Peri – Adriatic Area - Veli Lošinj (Croatia): Proceedings of the Workshop on Geothermal Energy.
Dewey, J.F., Helman, M.L., Knott, S.D., Turco, E., Hutton, D.H.W., 1989. Kinematics of the western Mediterranean. Geol. Soc. Lond., Spec. Publ. 45 (1), 265–283. https://doi.org/10.1144/gsl.sp.1989.045.01.15.
EMODnet Digital Bathymetry, 2018. EMODnet bathymetry consortium. Available at: https://www.emodnet.eu (Accessed September 14, 2018).
EU-DEM, 2017. Copernicus Land Monitoring Service. Available at: https://www.eea.europa.eu/data-and-maps/data/copernicus-land-monitoring-service-eu-dem.
European Commission, 2021. Mobility and Transport, Trans-European Transport Network TEN-T. Available at: https://ec.europa.eu/transport/themes/infrastructure/ten-t_en.
Faccenna, C., Becker, T.W., Auer, L., Billi, A., Boschi, L., Brun, J.P., Capitanio, F.A., Funiciello, F., Horvàth, F., Jolivet, L., Piromallo, C., Royden, L., Rossetti, F., Serpelloni, E., 2014. Mantle dynamics in the Mediterranean. Rev. Geophys. 52, 283–332. https://doi.org/10.1002/2013RG000444.
Fantoni, R., Franciosi, R., 2010. Tectono-sedimentary setting of the Po Plain and Adriatic foreland. Rend. Fis. Acc. Lincei 21, 197–209. https://doi.org/10.1007/s12210-010-0102-4.
Fantoni, R., Catellani, D., Merlini, S., Rogledi, S., Venturini, S., 2002. La registrazione degli eventi deformativi cenozoici nell'avampaese Veneto-Friulano. Mem. Soc. Geol. It. 57, 301–313.
Finetti, I., Del Ben, A., 2005. Crustal tectono-stratigraphic setting of the Adriatic Sea from new CROP seismic data. In: Finetti, I. (Ed.), CROP Project: Deep Seismic Exploration of the Central Mediterranean and Italy. Elsevier Science, pp. 519–547.
Fitzko, F., Suhadolc, P., Aoudia, A., Panza, G., 2005. Constraints on the location and mechanism of the 1511 Western-Slovenia earthquake from active tectonics and modeling of macroseismic data. Tectonophysics 404, 77–90.
Furlani, S., Biolchi, S., Cucchi, F., Antonioli, F., Busetti, M., Melis, R., 2011. Tectonic effects on Late Holocene sea level changes in the Gulf of Trieste (NE Adriatic Sea, Italy). Quat. Int. 232, 144–157.
Galadini, F., Poli, M., Zanferrari, A., 2005. Seismogenic sources potentially responsible for earthquakes with M ≥ 6 in the eastern Southern Alps (Thiene-Udine sector, NE Italy). Geophys. J. Int. 161, 739–762.
GEO-CGT, 2013. Carta geologica del Carso Classico scala 1:50.000 (Progetto GEO-CGT - Carta di sintesi geologica alla scala 1:10.000) and "Brevi Note Illustrative della Carta Geologica del Carso Classico Italiano" with the contribution of Cucchi F., Piano C., Fanucci C. F., Pugliese N., Tunis G. and Zini L. Regione Autonoma Friuli Venezia Giulia. Retrieved April 2016, from. http://www.regione.fvg.it/rafvg/cms/RAFVG/ambiente-territorio/tutela-ambiente-gestione-risorse-naturali/FOGLIA201/FOGLIA9/.
Giustiniani, M., Busetti, M., Dal Cin, M., Barison, E., Cimolino, A., Brancatelli, G., Baradello, L., 2022. Geophysical and geological views of potential water resources in the North-Eastern Adriatic Sea. Geosciences 12 (3), 139. https://doi.org/10.3390/geosciences12030139. MDPI.
Gordini, E., Marocco, R., Tunis, G., Ramella, R., 2004. I depositi cementati del Golfo di Trieste (Adriatico Settentrionale): Distribuzione areale, caratteri geomorfologici e indagini acustiche ad alta risoluzione. Il Quaternario. Italian J. Quat. Sci. 17 (2), 555–563.
Guidarelli, M., Aoudia, A., Costa, G., 2017. 3-D structure of the crust and uppermost mantle at the junction between the Southeastern Alps and External Dinarides from ambient noise tomography. Geophys. J. Int. 211 (3), 1509–1523. https://doi.org/10.1093/gji/ggx379.
Handy, M.R., Ustaszewski, K., Kissling, E., 2015. Reconstructing the Alps–Carpathians–Dinarides as a key to understanding switches in subduction polarity, slab gaps and surface motion. Int. J. Earth Sci. 104 (1), 1–26. https://doi.org/10.1007/s00531-014-1060-3.
IRDAT-FVG, 2017. Infrastruttura Regionale di Dati Ambientali e Territoriali per il Friuli Venezia Giulia. Available at: https://irdat.regione.fvg.it/WebGIS/.
Jurkovšek, B., Biolchi, S., Furlani, S., Kolar-Jurkovšek, T., Zini, L., Jež, J., Cucchi, F., 2016. Geology of the Classical Karst Region (SW Slovenia–NE Italy). J. Maps 12 (sup1), 352–362. https://doi.org/10.1080/17445647.2016.1215941.
Krabbenhoeft, A., von Huene, R., Miller, J.J., Klaeschen, D., 2021. Subducting oceanic basement roughness impacts on upper-plate tectonic structure and a backstop splay fault zone activated in the southern Kodiak aftershock region of the Mw 9.2, 1964 megathrust rupture, Alaska. Geosphere 17 (2), 409–437. https://doi.org/10.1130/GES02275.1.
Le Breton, E., Handy, M.R., Molli, G., Ustaszewski, K., 2017. Post-20 Ma motion of the Adriatic Plate: new constraints from surrounding orogens and implications for crust-mantle decoupling. Tectonics 36, 3135–3154. https://doi.org/10.1002/2016TC004443.
Liu, Y., Hubbard, J., Almeida, R.V., Foster, A., Liberty, L., Sin Lee, Y., Sapkota, S.N., 2020. Constraints on the shallow deformation around the Main Frontal Thrust in central Nepal from refraction velocities. Tectonophysics 777, 228–366. https://doi.org/10.1016/j.tecto.2020.228366.
Mavko, G., Mukerji, T., Dvorkin, J., 2009. The Rock Physics Handbook: Tools for Seismic Analysis in Porous Media. Cambridge University Press.
Meletti, C., Marzocchi, W., D'Amico, V., Lanzano, G., Luzi, L., Martinelli, F., Pace, B., Rovida, A., Taroni, M., Visini, F., Group, 2021 Mar. 15. MW (MPS19 Working Group), 2021. *The new Italian seismic hazard model (MPS19)*. Ann. Geophys. 64 (1), SE112. https://doi.org/10.4401/ag-8579.
Merlini, S., Doglioni, C., Fantoni, R., Ponton, M., 2002. Analisi strutturale lungo un profilo geologico tra la linea Fella-Sava e l'avampaese adriatico (Friuli Venezia Giulia-Italia). Mem. Soc. Geol. It. 57, 293–300.
Nicolich, R., Della Vedova, B., Giustiniani, M., Fantoni, R., 2004. Carta del Sottosuolo della Pianura Friulana e Note Illustrative. Regione Autonoma Friuli Venezia Giulia e Università degli Studi di Trieste, 32 pp.
OGS, 2014. CAT3D software (v6.0). Computer Aided Tomography for 3D models, User manual.
OGS, 2017. Bollettino della Rete Sismometrica del Friuli Venezia Giulia. Available at: http://www.crs.inogs.it/bollettino/RSFVG/.
Park, J.O., Tsuru, T., Takahashi, N., Hori, T., Kodaira, S., Nakanishi, A., Miura, S., Kaneda, Y., 2002. A deep strong reflector in the Nankai accretionary wedge from multichannel seismic data: Implications for underplating and interseismic shear stress release. J. Geophys. Res. 107 (B4) https://doi.org/10.1029/2001JB000262.
Patricelli, G., Poli, M.E., 2020. Quaternary tectonic activity in the north-eastern Friuli Plain (NE Italy). Boll. Geofis. Teor. Appl. 61 https://doi.org/10.4430/bgta0319, 24 pp.
Picotti, S., Dal Cin, M., Böhm, G., Busetti, M., 2018. Evidences of Seismic Flysch Anisotropy in the Gulf of Trieste. In: 24th European Meeting of Environmental and Engineering Geophysics. https://doi.org/10.3997/2214-4609.201802637. Sep 2018, 1–5.
Placer, L., Vrabec, M., Celarc, B., 2010. The bases for understanding of the NW Dinarides and Istria Peninsula tectonics. Geologija 53 (1), 55–86.
Poli, M., Monegato, G., Zanferrari, A., Falcucci, E., Marchesini, A., Grimaz, S., Del Pin, E., 2015. D6/a2.1 - Seismotectonic characterization of the western Carnic pre-alpine area between Caneva and Meduno (NE Italy, Friuli). Base-knowledge improvement for assessing the seismogenic potential of Italy. DPC-INGV-S1 Project.
Port Network Authority of the Eastern Adriatic Sea, 2021. Available at: https://www.porto.trieste.it/eng/port-authority/mission-eng.
Rebez, A., Santulin, M., Tamaro, A., Slejko, D., Sani, F., Martelli, L., Bonini, M., Corti, G., Poli, M.E., Zanferrari, A., Marchesini, A., Busetti, M., Dal Cin, M., Spallarossa, D., Barani, S., Scafidi, D., Barreca, G., Monaco, C., 2016. Seismogenetic zonation as a branch of the logic-tree for the new Italian Seismic Hazard Map - MPS16: a preliminary outline. In: Proceedings of the 35th Gruppo Nazionale di Geofisica della Terra Solida (GNGTS) Congress, Lecce, pp. 314–320. Available at: https://gngts.ogs.it/archivio/files/2016/S21/Riassunti/Rebez.pdf, 22-24 november 2016.
Rovida, A., Locati, M., Camassi, R., Lolli, B., Gasperini, P., 2020. The Italian earthquake catalogue CPTI15. Bull. Earthq. Eng. 18 (7), 2953–2984. https://doi.org/10.1007/s10518-020-00818-y.
Santulin, M., Tamaro, A., Rebez, A., Slejko, D., Sani, F., Martelli, L., Bonini, M., Corti, G., Poli, M.E., Zanferrari, A., Marchesini, A., Busetti, M., Dal Cin, M., Spallarossa, D., Barani, S., Scafidi, D., Barreca, G., Monaco, C., 2017. Seismogenic zonation as a branch of the logic tree for the new Italian seismic hazard map - MPS16: a preliminary outline. Boll. Geofis. Teor. Appl. 58 (4), 313–342. https://doi.org/10.4430/bgta0216.
Schmid, S.M., Fügenschuh, B., Kissling, E., Schuster, R., 2004. Tectonic Map and overall architecture of the Alpine orogeny. Eclogae Geol. Helv. 97, 93–117. https://doi.org/10.1007/s00015-004-1113-x.
Schön, J.H., 1996. Physical properties of rocks. Handbook of Geophysical Exploration. Pergamon Press.
Scrocca, D., Doglioni, C., Innocenti, F., Manetti, P., Mazzotti, A., Bertelli, L., Burbi, L., D'Offizi, S., 2003. CROP Atlas – Seismic Reflection Profiles of the Italian Crust. Memorie descrittive della Carta Geologica d'Italia 52, 193 pp., 71 plates.
Stewart, R.R., 1991. Exploration Seismic Tomography: Fundamentals. Society of Exploration Geophysicists, Tulsa (USA), p. 196.
Stipčevič, J., Tkalčič, H., Herak, M., Markušič, S., Herak, D., 2011. Crustal and uppermost mantle structure beneath the External Dinarides, Croatia, determined from teleseismic receiver functions. Geophys. J. Int. 185, 1103–1119.
TRANSALPWorking Group, 2002. First deep seismic images of the Eastern Alps reveal giant crustal wedges and transcrustal ramps. Geophys. Res. Lett. 29 (10) https://doi.org/10.1029/2002GL014911, 92-1–92-4.
Trobec, A., Busetti, M., Zgur, F., Baradello, L., Babich, A., Cova, A., et al., 2018. Thickness of marine holocene sediment in the Gulf of Trieste (Northern Adriatic Sea). Earth Syst. Sci. Data 10, 1077–1092. https://doi.org/10.5194/essd-10-1077-2018.
Van der Sluis, A., Van der Vorst, H.A., 1987. Numerical solutions of large, sparse linear algebraic systems arising from tomographic problems. In: Nolet, G. (Ed.), Seismic Tomography, D. Reidel Publishing Co., Dordrecht, Holland, pp. 49–83.
Vesnaver, A., 1994. Towards the uniqueness of tomographic inversion solutions. J. Seism. Explor. 3, 323–334.

Vesnaver, A., Böhm, G., 2000. Staggered or adapted grids for seismic tomography? Lead. Edge 19 (9), 944–950.
Vesnaver, A., Böhm, G., Cance, P., Dal Cin, M., Gei, D., 2020. Windowless Q-factor tomography by the instantaneous frequency. Geophys. Prospect. 68, 2611–2636. https://doi.org/10.1111/1365-2478.13020.
Vesnaver, A., Böhm, G., Busetti, M., Dal Cin, M., Zgur, F., 2021a. Broadband Q-factor imaging for geofluid detection in the Gulf of Trieste (northern Adriatic Sea). Front. Earth Sci. 9, 84. https://doi.org/10.3389/feart.2021.640194.
Vesnaver, A., Busetti, M., Baradello, L., 2021b. Chirp data processing for fluid detection at the Gulf of Trieste (northern Adriatic Sea). Bull. Geophys. Oceanogr. 62, 365–386. https://doi.org/10.4430/bgo00361.
Vičič, B., Aoudia, A., Javed, F., Foroutan, M., Costa, G., 2019. Geometry and mechanics of the active fault system in western Slovenia. Geophys. J. Int. 217 (3), 1755–1766. https://doi.org/10.1093/gji/ggz118.
ViDEPI-Project, 2009. Visibility of Petroleum Exploration Data in Italy. Available at: https://www.videpi.com.
Viscolani, A., Grützner, C., Diercks, M.L., Reicherter, K., Ustaszewski, K., 2020. Late quaternary tectonic activity of the Udine-Buttrio Thrust, Friulian Plain, NE Italy. Geosciences 10, 84. https://doi.org/10.3390/geosciences10020084.
Visini, F., Pace, B., Meletti, C., Marzocchi, W., Akinci, A., Azzaro, R., Barani, S., Barberi, G., Basili, R., Bird, P., Bonini, M., Burrato, P., Busetti, M., Carafa, M.M.C., Cocina, O., Console, R., Corti, G., D'Agostino, N., D'Amico, S., D'Amico, V., Dal Cin, M., Falcone, G., Fracassi, U., Gee, R., Kastelic, V., Lai, C.G., Langer, H., Maesano, F.E., Marchesini, A., Martelli, L., Monaco, C., Murru, M., Peruzza, L., Poli, M.E., Pondrelli, S., Rebez, A., Rotondi, R., Rovida, A., Sani, F., Santulin, M., Scafidi, D., Selva, J., Slejko, D., Spallarossa, D., Tamaro, A., Tarabusi, G., Taroni, M., Tiberti, M.M., Tusa, G., Tuvè, T., Valensise, G., Vannoli, P., Varini, E., Zanferrari, A., Zuccolo, E., 2021. Earthquake rupture forecasts for the MPS19 seismic hazard model of Italy. Ann. Geophys. 64 (2), SE220. https://doi.org/10.4401/ag-8608.
Vrabec, M., Fodor, L., 2006. Late Cenozoic tectonics of Slovenia: Structural styles at the northeastern corner of the Adriatic microplate. In: Pinter, N., Grenerczy, G., Weber, J., Medak, D., Stein, S. (Eds.), The Adria Microplate: GPS Geodesy, Tectonics, and Hazards. Nato Science Series: IV: *Earth and Environmental Sciences*, 61. Springer, pp. 151–168. https://doi.org/10.1007/1-4020-4235-3_10.
Weber, J., Vrabec, M., Pavlovčič-Prešeren, P., Dixon, T., Jiang, Y., Stopar, B., 2010. GPS-derived motion of the Adriatic microplate from Istria Peninsula and Po Plain sites, and geodynamic implications. Tectonophysics 483 (3–4), 214–222. https://doi.org/10.1016/j.tecto.2009.09.001.
Yilmaz, O., 2001. Seismic Data Analysis: Processing, Inversion and Interpretation of Seismic Data. Stephen M. Doherty - SEG, Tulsa.
Zampa, L.S., 2020. Technical Report 05/2020OGS. New bathymetric maps of the north east Adriatic Sea. Available at: https://www2.eecs.berkeley.edu/Pubs/TechRpts/.
Zanferrari, A., Bollettinari, G., Carobene, L., Carton, A., Carulli, G., Castaldini, D., Sauro, U., 1982. Evoluzione neotettonica dell'Italia nord-orientale. Mem. Sci. Geol. 35, 355–376.
Zanferrari, A., Avigliano, R., Monegato, G., Paiero, G., Poli, M.E., Barbieri, S., Zanolla, S., 2008. Note Illustrative della Carta Geologica d'Italia alla scala 1:50.000, foglio 066 Udine. Servizio Geologico; ISPRA - Servizio Geologico d'Italia 176.
Zanferrari, A., Masetti, D., Monegato, G., Poli, M., Avigliano, R., Carraro, F., Stefani, C., 2013. Carta geologica d'Italia alla scala 1:50.000 – Foglio 049 Gemona del Friuli – Note Illustrative. Regione Friuli Venezia Giulia - Servizio Geologico; ISPRA - Servizio Geologico d'Italia 262.
Zecchin, M., Busetti, M., Donda, F., Dal Cin, M., Zgur, F., Brancatelli, G., 2022. Plio-Quaternary sequences and tectonic events in the northern Adriatic Sea (northern Italy). Mar. Pet. Geol. 142 https://doi.org/10.1016/j.marpetgeo.2022.105745.
Zelt, C.A., Smith, R.B., 1992. Seismic travel-time inversion for 2-D crustal velocity structure. Geophys. J. Int. 108, 16–34.
Zgur, F., Codiglia, R., Busetti, M., Petronio, L., De Vittor, R., Loreto, M., Romeo, R., 2010. Studio dell'evoluzione geologica e tettonica del Golfo di Trieste (Adriatico Settentrionale). *OGS report 2010/24 RIMA 6 ADEST* dd. 18-03-2010(24), 50 pp.
Zgur, F., Facchin, L., Busetti, M., Vrabec, M., Slavec, P., Romeo, R., Pelos, C., 2013. Correlation of tectonic structures occurring onland in the Istria Peninsula and in the Gulf of Trieste (Northern Adriatic), and investigation of their neotectonic Activity. *OGS report 2013/64 IRI 9 ADEST* dd. 02/07/2013(64), 51 pp.